NTNU

Norwegian University of
Science and Technology

Ferromagnetic Resonance of LSMO Thin Film

Godfred Inkoom

Condensed Matter Physics
Submission date: May 2011
Supervisor: Erik Wahlstrøm, IFY

Norwegian University of Science and Technology
Department of Physics

FERROMAGNETIC RESONANCE OF LSMO THIN FILM

A thesis submitted to the Department of Physics
Norwegian University of Science and Technology, Norway

In partial Fulfillment of the Requirements for the
Degree of Master of Science in Physics

By
Godfred Inkoom

Norwegian University of Science and Technology, Norway
May 2011

NORWEGIAN UNIVERSITY OF SCIENCE AND TECHNOLOGY,
NORWAY
DEPARTMENT OF
PHYSICS

The undersigned hereby certify that they have read and recommend to the Faculty of Natural Science and Technology for acceptance a thesis entitled " **FERROMAGNETIC RESONANCE OF LSMO THIN FILM**" by **Godfred Inkoom** in partial fulfillment of the requirements for the degree of **Master of Science**.

Advisor: _____
Associate Prof. Erik Wahlström

This work is dedicate

To My Late Father Mr. Raymond Incoom

Table of Contents

List of Figures

Abstract

The magnetic properties of a 15uc thick LSMO thin film on $SrTiO_3$ (STO) substrate at T=150K was investigated using the technique of ferromagnetic resonance (FMR). The FMR measurement of the 15uc thick LSMO thin film at a frequency $f = 9.75GHz$ and power $P = 0.6325mW$ as a function of the angle ψ between the static magnetic field H, and the easy direction of magnetization within the sample plane in the "in-plane" (IP) configuration displayed an FMR spectrum. This resonance spectrum shows unequal resonance field peaks. The unequal peaks in the resonance field may be attributed to the uniaxial anisotropy field which satisfies the conditions for ferromagnetic resonance. The unequal peaks in the resonance field shows a maximum and minimum with negative and positive curvature which either increases or decreases with respect to the resonance field respectively. This increase or decrease in the resonance field depends on the magnetization direction. It has been shown that for a thick 15uc LSMO thin film at $T = 150K$ the center position and the full width half maximum (FWHM) of the resonance field were 1070.1875 Oe and 159.3125 Oe respectively.

Acknowledgements

The lord has been good to me and so my thanks go to Him for all He has done, especially for his strength and mercies which enabled me complete this work. I am most grateful to my supervisor Associate Prof. Erik Wahlström for his guidance, suggestions and constructive criticisms towards the completion of this work. I am also most grateful to the Norwegian government for their financial support through the Quota Scheme. I would personally thank Asmund (PhD student) for his encouragement throughout the experimental work and Snorre Hansens (student advisor); in charge of international master students in condensed matter physics. Finally I want thank all my family members and anyone who has contributed in one way or the other to the successful completion of this work.

Chapter 1

INTRODUCTION

1.1 MOTIVATION AND OBJECTIVES

Thin films have been a topic of much interest and importance over the last decades. With the current drive towards greater data storage densities in computer disk drives, microelectronics and low field sensors, attention is being focused on the magnetic properties of these films. The technique of FMR can therefore be used for the study of the magnetic properties of thin films.

Ferromagnetic resonance is one of such most powerful experimental techniques which can be used for the study of magnetic properties of thin films as a result of its high sensitivity and high resolution. With ferromagnetic resonance, essential parameters describing magnetic properties of thin films such as the effective magnetization, magnetization density, magnetic anisotropy, spin relaxation time, intrinsic α-Gilbert damping constant, the spectroscopic splitting factor (which provides information on the orbital contribution to the magnetic moment) and the ferromagnetic resonance linewidth (which provides a means of measuring damping in especially magnetic materials) can be determined.

The objectives of this current thesis is to determine the ferromagnetic resonance of a 15uc thick LSMO thin film. LSMO is the most researched and studied colossal magnetoresistant manganite. Data which were obtained from the experiment were then plotted in Matlab

and based on the plot the width and center position of the FMR spectrum of the 15uc thick LSMO thin film at $T = 150K$ was calculated.

1.2 BRIEF HISTORY OF MAGNETISM AND FERROMAGNETIC RESONANCE

The quest for an answer to what magnetism is and why the magnet has the ability to attract ferrous objects has fascinated many people including Thales of Miletus (about 634-546 BC) and the young Albert Einstein [11,2]. Thales of Miletus described magnetism as the attraction of iron by " lodestone", which is a naturally occurring mineral of magnetite, Fe_3O_4 [2]. According to Phiny's account about the history of magnetism, the magnet stone was named after its discoverer, Magnes whiles he was pasturing his flock and the tip of his iron-nailed shoes stuck a "magnetick" field [3,2].

The origins of magnetism lie in the properties of the electrons as explained by the laws of quantum physics [11]. Magnetism can be explained by using the concepts of spin which gives rise to the spin magnetic moment, the motion of electronic charges and the orbital magnetic moment [2]. Part of an electron's magnetic properties (spin magnetism) results from its quantum mechanical spin state, while another part results from the orbital motion of electrons around an atom's nucleus (orbital magnetism) and from the magnetism of the nucleus itself (nuclear magnetism) [11,2].

The history of magnetism dates back to the Chinese in 2500BC, and to the Greeks as far as 600BC and during those era, magnetic materials were classified into three main types, namely; para, dia and ferromagnetics [1] and in order to have some theoretical understanding about these class of magnetic materials, concepts from electromagnetism and atomic theory was needed [1]. It was electromagnetism which brought about the unification of electricity and magnetism and the ideas from electromagnetism showed that moving charges produce

magnetic fields [1]. The theory of diamagnetism was explained using the idea of the Lorentz force

$$F_L = q[E + (\frac{1}{C})V \times H] \tag{1.2.1}$$

on an electron which is orbiting when a magnetic field H was applied [1] and paramagnetism was explained using the idea that atoms or molecules possess a permanent dipole moments and these permanent dipole moments arise as a result of the fact that every orbiting electron in a current loop acts like a tiny magnetic shell [1]. The Lorentz force, F_L gives the force acting on a charge q moving with a velocity V which is subjected to an electric field, E and a magnetic field, H. At the atomic level, it was really difficult for an explanation and understanding of ferromagnetism but through the research work by Heisenberg in 1920 in quantum mechanics a new door opened for the understanding of such an important phenomenon [1].

Classical electromagnetism was at its peak when research works were carried out by Michael Faraday (1791-1867) and James Clerk Maxwell (1831-1879) [2]. In 1831 and 1845, Michael Faraday discovered both the electromagnetic induction and the direct connection between magnetism and light [2]. The direct connection between magnetism and light was placed on a firm foot mathematically by Maxwell through the studies of equations describing both the electric and magnetic fields [2]. This led to his famous conclusion that [2]

$$C = \frac{1}{\sqrt{\mu_o \varepsilon_o}} \tag{1.2.2}$$

and that light is a form of an electromagnetic wave which travels with the speed of light C. The magnetic and the electric fields together form the two components of electromagnetism [11].

There are several reasons why magnetism is such an important branch of physics and some of the reasons include the following. Firstly, it can be said that over the last 2500 years,

magnetism has been applied in the field of navigation, power production, and " high tech" applications [2]. Currently, the permanent magnets has found its way in areas including; high-tension magnetos, telephone generators, telephone receivers, gramophone pick up units, moving-coil loudspeakers, television focus units and other equipments involving deflection of electron beams, electricity meters and thermostats [4]. Secondly, of all the four forces in nature; electromagnetism, strong interaction, weak interaction and gravitation, the electromagnetic force is considered to be the greatest and it forms the basics of contemporary physics [2]. Thirdly, the field of magnetism is constantly undergoing dynamic developments and is also one of fastest forefront research areas in physics because of the ever increasing desire for " smaller and faster " devices [2]. For instance, in the 1980s and 1990s a number of important discoveries in the field of magnetism were made [5]. Some of these include; interface anisotropies and the interlayer exchange coupling mechanism [5]. Currently, the field of magnetism is driven by vitality as a result of new discoveries in this area of research [2] and it was not a surprise to the physics community when the 2007 Noble Prize in Physics was awarded to Albert Fert and Peter Grünberg for their discovery of giant magnetoresistance (GMR) effect in multilayers alternating a ferromagnetic metal with a non-magnetic metal (e.g Fe/Cr or Co/Cu) [12].

Ferromagnetic resonance (FMR) is a basic technique which is used for the study of the forces that determine the dynamical properties of magnetic materials [14]. This technique of ferromagnetic resonance was discovered by Griffiths (1946) but the theory of the resonance effect was proposed by Charles Kittel (1947) [15]. The main outcome of Kittel's theory was that, the resonance condition for a plane surface should be

$$\omega_o = \gamma\sqrt{BH} \tag{1.2.3}$$

instead of the Larmor condition

$$\omega_o = \gamma H \tag{1.2.4}$$

[15]. Since the discovery of FMR, the technique has been applied in so many research works including the determination of the g-factor, the magnetic anisotropy constant and the interlayer magnetic coupling of films and multilayers [16]. FMR has also been used in the study of superlattice and single films of few layers capped with a non-magnetic metal layer [17]. In the field of FMR spectroscopy also, the technique of FMR can provide information on the magnetic damping through the study of the linewidth of the absorption peak [18].

1.3 FERROMAGNETISM IN METALS

The phenomenon of ferromagnetism is characterized by a spontaneous magnetization even in the absence of an applied external field [6,1]. At temperature (T=0) all the magnetic moment are aligned parallel and this is as a result of the exchange interaction [6]. For the elemental transition metals, only cobalt, iron and nickel are ferromagnetic whereas chromium and manganese are antiferromagnetic [7]. In the periodic table also, metals in the second and third transition series and those of the isoelectronic to the magnetic members of the first series are not ferromagnetic [7].

Ferromagnetism in the elemental transition metals such as Fe, Ni, and Co occurs as a result of the delocalized conduction electrons from the narrow 3d band [7,13] and also as a result of the strong intraatomic interaction [8]. In metals, ferromagnetism occurs when the susceptibility diverges spontaneously (Stoner criterion). The Stoner criterion is roughly true for Fe, Co and Ni [9,11]. Although the Stoner criterion chalked some success, it failed in the explanation for the Pauli paramagnetism above the transition temperature and also the prediction of the destruction of ferromagnetism at the Stoner temperature(T_s) [9]. In the case of the Pauli type paramagnetism above the transition temperature, the model fails because of the fact that ferromagnets display a Curie-Weiss susceptibility in the paramagnetic phase [9]. On the prediction of the destruction of ferromagnetism, the Stoner model predicts higher temperature for the Stoner temperatures (T_s) than the Curie

temperature (T_c) [9]. This in reality might not be true because the orientation of the moments fluctuates critically at the Curie temperature [9] and that, ferromagnetism usually occurs below the Curie temperature. For iron, cobalt and nickel, the Stoner temperatures predicted by the Stoner model were 6000K, 4000K and 2900K [9] respectively whiles the Curie temperatures for iron, colbalt and nickel are 1028K, 1393K and 631K respectively [10].

1.4 OUTLINE OF THESIS

This work consists of five main chapters. The first chapter provides the motivation and objectives of the work and also a brief history about magnetism and ferromagnetic resonance. This chapter also gives a brief explanation of ferromagnetism in metals. The theoretical aspect is discussed in the second chapter. Other issues to be addressed in this chapter include; magnetocrystalline anisotropy, shape anisotropy, magnetic surfaces and interface anisotropies, damping in magnetic ultrathin films, LSMO, and some potential applications of the mixed valence manganites and LSMO. In the third chapter, the methodology describing how the experimental work was carried out is discussed. The fourth chapter focuses on the results and discussions. The conclusions and recommendations derived from the experiment are outlined in the fifth chapter. This chapter is followed by the bibliography and list of abbreviations and constants.

Chapter 2

THEORETICAL CONSIDERATION

In this chapter, a brief review of the important theoretical aspects of the work is presented. This includes; magnetization in ultrathin magnetic films, magnetic anisotropies in thin films, shape anisotropy, magnetocrystalline anisotropy, magnetic surfaces and interface anisotropies, Landau-Lifshitz-Gilbert (LLG) equation, ferromagnetic resonance, damping in ultrathin magnetic thin films, LSMO and some potential applications of the mixed valence manganites and LSMO.

For magnetization in ultrathin magnetic films, the concept is that there is a loss of the internal degree of freedom in the ultrathin films. This then results in the exchange coupling in the ferromagnetic layer being excited by a uniform applied magnetic field. In shape anisotropy, the magnetization is affected by the macroscopic shape of the solid. For magneto crystalline anisotropy, the magnetization is oriented along some specific crystalline axes. Surface and interface anisotropies occurs as a result of the broken local symmetry which is due to the contribution of the surface energy which depends on the orientation of the magnetization on the surface. The LLG equation is a classical equation for the rate of change of the magnetization which can be used in the study of dispersive theory of magnetization in ferromagnets. Ferromagnetic resonance occurs as a result of the precession of the atoms

under a magnetic field.

2.1 MAGNETIZATION IN ULTRATHIN MAGNETIC FILMS

Intrinsic properties such as magnetization, Curie point, anisotropy and magnetostriction in thin films may differ from their bulk counterparts. This differences can be attributed to the special environments of the surface and the interface atoms and also as a result of the strain which is induced by the substrate [11]. For instance vanadium and rhodium become ferromagnetic in thin films which is 1-2 monolayer thick whiles their bulk counterpart is nonmagnetic [11]. In the case of ultrathin films, the ultrathin layer looses its internal degree of freedom and since the exchange coupling in the ferromagnetic layer is excited by the uniform applied magnetic field in the film plane, the magnetic moments across the film is nearly parallel [5].

2.1.1 MAGNETIC ANISOTROPY IN THIN FILMS

Ferromagnetic materials usually have two directions of magnetization, namely; the "easy" and the "hard " directions [20]. The amount of energy which is required to rotate the magnetization direction from the preferred axes (easy axes) into the hard direction is called the magnetic anisotropy energy [2]. In thin films, some of the sources of anisotropy includes; surface and mechanical strain or stress [11]. Surface anisotropy arises as a result of the coupling between the surface atoms to the crystal field which is produced from the anisotropic environment [11]. The magnetic anisotropy energy (MAE) is only a few tens of $\mu eV/atom$ of the total energy of the atom [19].

Technologically, magnetic anisotropy is one of the important properties of magnetic materials. This is because depending on a material's application, a decision is made whether to use a material with high, low or medium magnetic anisotropy [20]. Typical example is the ferromagnetic thin films which has a high anisotropy which is used in modern perpendicular

magnetic recording technology with a density storage of 1 $Tbits/in.^2$ [21] .

There are other sources of magnetic anisotropy, namely; the magnetic dipolar interaction and the spin-orbit coupling [20]. The absence of these two other sources of anisotropy means that the total energy of the electron-spin system does not depend on the direction of the magnetization [20]. The spin-orbit coupling which is considered as a weak relativistic interaction which is responsible for Hund's rule is the physical origin of magnetic anisotropy, magnetocrystalline anisotropy, anisotropic magnetoresistance and spin Hall effect [21,11].

The magnetic anisotropy energy and the orbital momentum are related to the Hamiltonian and the spin orbit coupling by [21,24]

$$H = \xi L \cdot S \tag{2.1.1}$$

where ξ is the spin orbit coupling. The anisotropy energy density, E_{ani} which is rotationally symmetric with respect to the easy axis and also depends on the relative orientation of the magnetization with respects to its axis can be expressed as a series expansion of the form [2]

$$E_{ani} = K_1 sin^2\psi + K_2 sin^4\psi + K_3 sin^6\psi + ... \tag{2.1.2}$$

Where $K_i (i = 1, 2, 3, ...)$ are the anisotropy constants and ψ is the angle between the magnetization and the magnetic axis [2]. In the case of thin films, $K_1 \gg K_2$ and also K_3 which means that Eq.(2.1.2) can be rewritten as [2]

$$E_{ani} = K_1 sin^2\psi \tag{2.1.3}$$

When Eq.(2.1.3) is differenciated with respect to ψ and equated to the effective torque

$$\tau_{eff} = M \times H_{ani} \tag{2.1.4}$$

this yields

$$H_{ani} = \frac{2K_1 cos\psi}{M} \tag{2.1.5}$$

The above equation, (2.1.5) for the anisotropy field means that the field stimulates a preferred axis since it changes sign when ψ goes through $\frac{\pi}{2}$ [2]. The anisotropy constant, K_1 can be expressed as a sum of the shape anisotropy (K_s) and the magnetocrystalline anisotropy (K_u). When $K_1 > 0$ it means that the film prefers to be magnetized perpendicular to its plane and when $K_1 < 0$, it means that the easy direction will be in the plane of the thin film [2].

The magnetic anisotropy of LSMO thin film which was deposited onto STO (110) substrate was first studied by Suzuku et. al (1997). Suzuki and his coworkers observed that the in-plane uniaxial behavior of the LSMO thin film which was deposited onto the STO substrate with the easy axis was aligned with the [001] crystal direction [154]. Some of the important magnetic anisotropies such as shape anisotropy, magnetocrystalline anisotropy and surface and interface anisotropies are discussed in the next section.

SHAPE ANISOTROPY

Shape anisotropy usually arises as a result of the anisotropy of the demagnetizing field, H_d due to the long-range dipolar interaction in the particle [11,22]. The relation between the demagnetizing field, H_d and the magnetization, M is expressed as [11]

$$H_d = NM \tag{2.1.6}$$

where N is the demagnetizing factor. The demagnetizing factors are different for different samples with different geometrical shapes and magnetization direction [11]. For instance, a thin film with magnetization direction parallel or perpendicular to it's plane has demagnetizing factor of 0 or 1 respectively, whiles a sphere whose magnetization direction is in any direction has a demagnetizing factor of $\frac{1}{3}$ [11]. In the macroscopic limit, the dipole-dipole contribution to the magnetic anisotropy is called shape anisotropy (K_s)[23].

For homogeneous films, the shape anisotropy can be expressed as [23]

$$K_s = -2\pi M_s^2 \tag{2.1.7}$$

where M_s is the saturation magnetization whiles in the case of multilayer films, one uses the same expression for the shape anisotropy as in the homogeneous films but the saturation magnetization is replaced by its average value, $\overline{M_s}$ [23]. The shape anisotropy is also quadratic in magnetization since it can be diagonalized [22].

Inside an infinite system, the relation

$$B = \mu_o(H + M) \tag{2.1.8}$$

holds unlike a situation where we have a finite sample which possess poles at its surface and this leads to a stray field outside the sample [6,2]. The stray field can be expressed as $H_s = \frac{1}{\mu_o}B$ [2]. The occurrence of this stray field leads to a demagnetization field inside the sample [6]. The stray field energy, E_{str} can be expressed as [11,6]

$$E_{str} = -\frac{1}{2}\int \mu_o M H_d dV \tag{2.1.9}$$

where H_d is the demagnetizing field inside the sample. Since a sphere has demagnetizing factor of $\frac{1}{3}$ [11], it means that the stray field energy density is

$$E_{str} = \frac{1}{6}\mu_o M^2 \tag{2.1.10}$$

and for an infinitely long cylinder, the stray field energy density is

$$E_{str} = \frac{1}{4}\mu_o M^2 sin^2\theta \tag{2.1.11}$$

[6,11]. For very thin plate, thin magnetic film and multilayer films, the stray energy density can be expressed as [6,24,20]

$$E_{str} = \frac{1}{2}\mu_o M^2 cos^2\theta \tag{2.1.12}$$

The stray field energy density for thin magnetic films and multilayers can also be rewritten as [6]

$$E_{str} = K_o + \chi sin^2\theta \tag{2.1.13}$$

Equation (2.1.13) means when $\theta = 90^0$ the stray field energy reaches its minimum value [6].

MAGNETOCRYSTALLINE ANISOTROPY

The search for the understanding of the origin of magnetocrystalline anisotropy started many years even before 1960 [24] and according to Van Vleck, the main origin of the magnetocrystalline anisotropy is as a result of the relativistic spin-orbit interaction of the electrons [24,6,2,22] and the crystal field interactions [11]. In the spin-orbit interaction, the electron orbitals are closely linked to the crystallographic structure and due to the interaction with the spins, they make the later prefer to align along a well-defined crystallographic axes [6]. Which means that for a magnetic material there are certain directions in space that are easier to magnetize than other directions and this is very useful for the designing of new materials for information storage [6,25]. In addition to the crystal field interaction and the relativistic spin-orbit interaction, the exchange interaction and the dipolar interaction can also contribute to the magneto crystalline anisotropy[20]. The difference between the exchange interaction and the dipolar interaction is that, the exchange interaction is independent of the angle between the spins and the crystal axes whiles the dipolar interaction depends on the orientation of the magnetization relative to the crystal axes [20].

Currently, an understanding of the magnetocrystalline anisotropy can be obtained from the ab initio bandstructure calculations[20] and a typical example of such calculation was carried out by Daaldrop(1991), where he concluded that the symmetry of the state determines whether or not the state split if the direction of magnetization is perpendicular or parallel to the film plane [20].

In magnetocrystalline anisotropy, the magnetization process is different when the magnetic field is applied along different crystallographic directions and this anisotropy reflects the crystal symmetry of the particular crystal system which is under consideration [11]. Since the magnetic anisotropy energy (MAE) can be defined as the amount of work which is needed to rotate the magnetization from the easy to the hard direction [2], it means that if this rotation is carried out at constant temperature, then the magnetocrystalline anisotropy energy can be also be defined as the change in the free energy ΔF. When we consider a closed system, thus a system in which there is no exchange of particles between the system and its surrounding, it means that

$$dF = dW - SdT \tag{2.1.14}$$

where W is the workdone, S is the entropy and T is the temperature which is constant, then it means that

$$dF = dW \tag{2.1.15}$$

and that

$$\Delta F = F_2 - F_1 = \int_1^2 dW_{MAE} = MAE \tag{2.1.16}$$

where 1 and 2 denotes the initial and the final directions of the magnetization. This magnetization is usually determined by the anisotropy as a result of the exchange interaction which aligns the magnetic moment in a parallel direction [6]. The direction of magnetization which is expressed as [6]

$$m = \frac{M}{\mid M \mid} \tag{2.1.17}$$

relative to the coordinates axes can also be expressed by the directional cosines, α_i as $m = (\alpha_1, \alpha_2, \alpha_3)$ where

$$\alpha_1 = sin\theta cos\phi \tag{2.1.18}$$

$$\alpha_2 = sin\theta sin\phi \tag{2.1.19}$$

$$\alpha_3 = cos\theta \tag{2.1.20}$$

These three equations for the directional cosines also satisfies the condition that [6]

$$\alpha_1^2 + \alpha_2^2 + \alpha_3^2 = 1 \tag{2.1.21}$$

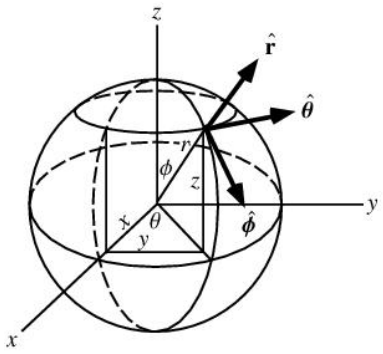

Figure 2.1: Spherical coordinates system which is used for calculating directional cosines. Adopted from ref.[118]

The magnetocrystalline energy per unit volume, E can be written as a power series expansion of the components of the magnetization as [6]

$$E = E_o + \sum_i b_i\alpha_i + \sum_{ij} b_{ij}\alpha_i\alpha_j + \sum_{ijk} b_{ijk}\alpha_i\alpha_j\alpha_k + \sum_{ijkl} b_{ijkl}\alpha_i\alpha_j\alpha_k\alpha_l + 0(\alpha^5) \tag{2.1.22}$$

For cubic systems, the energy density can be written as [6]

$$E = K_0 + K_1(\alpha_1^2\alpha_2^2 + \alpha_1^2\alpha_3^2 + \alpha_2^2\alpha_3^2 + K_2\alpha_1^2\alpha_2^2\alpha_3^2 + K_3(\alpha_1^2\alpha_2^2 + \alpha_1^2\alpha_3^2 + \alpha_2^2\alpha_3^2 + ...) \tag{2.1.23}$$

For the tetragonal systems, the energy density can be written as [6,140]

$$E = K_o + K_1cos^2\theta + K_2cos^4\theta + K_3sin^4\theta(sin^4\phi + cos^4\phi) \tag{2.1.24}$$

and for hexagonal system, the energy density can be expressed as [140]

$$E = K_1 sin^2\theta + K_2 sin^4\theta + K_3 sin^6\theta + K_3' sin^6\theta cos6\phi \tag{2.1.25}$$

where θ is the angle between the magnetization and the z-axis and ϕ is the azimuthal angle. These two angles, θ and ϕ can also be referred to as the polar angles of the magnetic moment in the crystal axis frame [140]. Similar expressions can also be derived for other crystal systems such as the orthorhombic systems[6]. The relations for the anisotropy can also be expressed as a set of orthonormal spherical harmonics with anisotropy coefficient K_l^m and the crystal field coefficient A_l^m as [11]

$$E = \sum_{l=2,4,6} K_l^m A_l^m Y_l^m(\theta, \phi) \tag{2.1.26}$$

.

SURFACE AND INTERFACE ANISOTROPIES

Surfaces and interface anisotropies are one of the most important magnetic anisotropies [6]. The concepts of magnetic surface anisotropy (MSA) was predicted theoretically by Néel(1954) [26,30,31,32,28]. Research interest in the area of magnetic properties of surfaces and interfaces took a center stage in the early part of the 1970s [26]. This intense interest was motivated by the need to understand the influence of "defects" such as surface on the formation of the properties of surface layer [26]. Some other important reasons why much effort was concentrated on the magnetic properties of surfaces and interfaces was as a result of its applications in devices especially the ultrathin magnetic films [27] and also the connection between the magnetic surfaces and interfaces to the magnetic oligatomic films and artificial superstructures [28]. One of the excellent tools which is used for the experimental analysis of magnetic surface anisotropies is the torsion oscillation magnetometry (TOM) which provides quantitative data on the magnetic surface and out-of-plane anisotropy of an ultrathin film with monolayer resolution [29].

Magnetic anisotropies come about as a result of the broken local symmetry due to the contribution of the surface energy which depends on the orientation of magnetization on the surface [30,28,33,6,55]. Néel proposed that the surface energy, σ_s is related to the angle, β between the magnetization, M and the surface normal, n by considering only the leading term [28]. This surface energy is expressed as [28]

$$\sigma_s = K_s cos^2\beta \tag{2.1.27}$$

where K_s is the out of plane magnetic surface anisotropy (MSA). Gradmann et.al later proposed an additional term, $K_{s,p} sin^2\beta cos^2\varphi$ to this surface energy by taking into account the polar coordinates β and the azimuthal angle φ in the plane of the film, where $K_{s,p}$ is a constant of the in-plane MSA and is independent of K_s [28].

Experimentally, the magnetic surface anisotropy can be determined from the study of thin film anisotropies as a function of the thickness of the thin film [31] and due to the broken symmetry at the interfaces, the effective anisotropy constant is expressed as [34,6]

$$K^{eff} = K_v^{eff} + \frac{2K_s^{eff}}{t} \tag{2.1.28}$$

where K_v^{eff} is the effective volume anisotropy constant and K_s^{eff} is the interface anisotropy constant and the factor 2 is as a result of the creation of two surface. Charppert and Bruno later revealed that the value of K_s^{eff} might not be purely due to the surface term but might also contain a volume magnetostatic term as result of an epitaxial strain which is induced on the thin film [35].

2.1.2 LANDAU-LIFSHITZ -GILBERT (LLG) EQUATION

When a magnetic dipole moment, μ is subjected to a magnetic field, H it experiences a torque, τ. The equation of motion is described as [36,37,2,41,132]

$$\frac{d\mu}{dt} = -\gamma(\mu \times H_o) \tag{2.1.29}$$

$$\frac{dM}{dt} = -\gamma(M \times H_{eff}) \tag{2.1.30}$$

where $\gamma = \frac{ge}{2mc}$ is called gyromagnetic ratio.

For a ferromagnetic material with majority of the electrons pointing their spin in a certain common direction usually below a certain temperature range as high as 1000K [37], the effective field, H_{eff} is unknown and can be expressed as the sum of several anisotropic field contributions (dipole, spin orbit, external and microwave) [36].

In studying the dispersive theory of magnetization of ferromagnets, Landau-Lifshitz (LL)(1935) proposed the equation of ferromagnetic spin chain which is an important magnetization equation, called Landau-Lifshitz (LL) equation. This LL equation is a classical theory for the rate of change of magnetization as a function of space and time under the application of an effective local field, H_{eff} with the effect of damping term included [41]. The LL equation is expressed as [42,11,2]

$$\frac{dM}{dt} = -\gamma[M \times \mu_o H_{eff}] - \frac{\lambda}{M_s^2}[M \times (M \times \mu_o H_{eff})] \tag{2.1.31}$$

where λ is the damping term which is sometimes referred to as the relaxation frequency[42,6]. The first term in the Landau- Lifshitz(LL) equation describes the torque on the magnetization vector which is exerted by the effective field, H_{eff} and the second term describes the damping torque which reorient the magnetization vector towards the effective field [42]. The LL equation describes both the evolution of spin fields in ferromagnets and also the precession of the magnetization in an effective field [43,44].

In 1954, Gilbert modified the Landau-Lifshitz (LL) equation based on the idea of the Lagrangian and this equation became known as the Landau-Lifshitz-Gilbert (LLG) equation [41]. The LLG equation can be expressed as [36,39,38,18,2,40,45,46,41,68,131,60,67,55,17,134,50,142,143]

$$\frac{dM}{dt} = -\gamma[(M \times H_{eff})] + \frac{G}{\gamma M_s^2}[M \times \frac{dM}{dt}] \tag{2.1.32}$$

where $\alpha = \frac{G}{\gamma M_s}$, γ is the gyromagnetic ratio and G is the Gilbert damping term which is also the relaxation rate per second [45,5]. The first term on the right hand side of the LLG equation is the precessional torque and the second term represents the Gilbert damping torque [38,18,39,45,46,67]. This LLG equation can be deduced from the lattice spin Hamiltonian by choosen an appropriate Poisson bracket [41]. The LLG equation which is valid for small magnetization motions [68] is a modification of Eq. (2.1.30) when the effect of damping is included. It can be observed from Eq. (2.1.31) and Eq. (2.1.32) that the precession term in the LL equation, $M \times \mu_o H_{eff}$ is replaced by $\frac{dM}{dt}$ in the LLG equation . The LLG equation can be transformed into the LL equation by using the transformation that $\Lambda = \frac{\gamma}{1+\gamma^2}$ and $\lambda = \frac{\alpha\gamma M_s}{1+\alpha^2}$ [42,48].

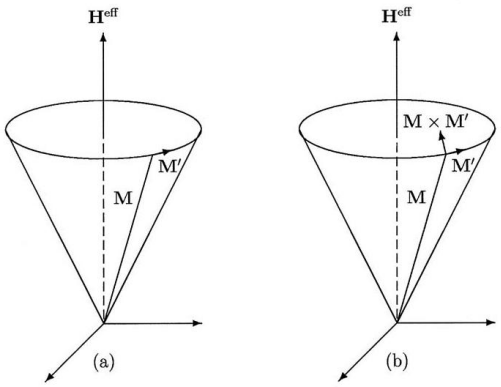

Figure 2.2: Magnetization precission (a) without damping and (b)with damping. Adopted from ref.[48,41]

Since the inception of the LLG equation it has been applied in many research fields including the interpretation and prediction of some experiments including domain wall structure, magnetization reversal and magnetic noise [49]. It has also been established that the LLG equation has some close relationship with other physical systems including the motion of a vortex filament, motion of curves and surfaces and the σ models in particle physics [41]. In

the area of magnetic devices also such as the random access memory (MRAM), the Gilbert damping coefficient has a close relation to the speed of switching a bit of information which is encoded by magnetization direction of a ferromagnetic grain and the energy demands of switching [50]. The quest for designing new materials for various applications can be more successful when more research works are carried out on the Gilbert damping mechanisms especially in the metallic ferromagnets [50].

Although the LLG equation has chalked some successes as a result of the fact it captures essential features of the dynamics of magnetization which occurs in condensed matter systems, there are many problems which still remain unsolved[68]. On the experimental front, the prediction of the α term in the LLG has been challenging due to insufficient nature of experimental data [68]. Theoretically, the main challenge in the LLG equation has been the derivation of the damping term and this is attributed to the fact that the damping term in various kinds of relaxation processes are melded together in a single damping term [68].

There are also other forms of phenomenological damping term which is found in other literature apart from the Gilbert damping term. Typical example is the Landau-Lifshitz (LL) term which is expressed as $\frac{-\lambda}{\gamma M_s^2}(M \times [M \times H_{eff}])$ where λ is the Landau-Lifshitz (LL) term [5]. For small damping, $\frac{G}{\gamma M_s} \ll 1$, the Gilbert relaxation torque and the Landau-Lifshitz relaxation terms, $\frac{-G}{\gamma M_s^2}[M \times (M \times H_{eff})]$ are equivalent [38,5].

2.1.3 FERROMAGNETIC RESONANCE

Ferromagnetic resonance (FMR) is an experimental technique which is used for the study of the magnetic properties of ultrathin films and magnetic thin films [51,17,132]. The origin of ferromagnetic resonance is as result of the precession of the atoms under a magnetic field, H[36]. The theory of ferromagnetic resonance effect was developed classically by C. Kittel (1947) and also within quantum mechanical framework by D. Polder (1948) [52]. In a typical ferromagnetic resonance experiment, a ferromagnetic material is irradiated in

an applied field with microwaves, where the applied field is swept at a fixed frequency [53,18,122,39]. In order for precession to be observed in FMR, a high frequency radiation usually in the GHz range must penetrate the sample and the resulting wavelength must be greater the size of the sample [11]. For example, a frequency, f = $10GHz$ results in $\lambda = 3cm$ so that this condition is satisfied for a millimeter size sample [11]. Also, the motion of the magnetization of ultrathin films such as LSMO in an FMR satisfies the condition that the wavelength involved is greater as compared to the lattice constant [128]. Typical value includes, frequency, f = $9.75GHz$ which is the X-band microwave frequency which yields in a wavelength $\lambda = 3.1cm$ which is greater as compared to the lattice constant of LSMO, $a = 0.388nm$ at room temperature.

The phenomenon of resonance can be described by applying a macroscopic equation of motion to the behavior of the magnetization, M which is formed by the magnetic moments, μ in the sample[54]. The magnetization, M is defined as [55,2,56]

$$M = \frac{\mu}{V_o} \tag{2.1.33}$$

where μ is the magnetic moment per atom and V_o is the atomic volume. For a single-domain magnetic film with thickness below the ultrathin film limit, the magnetization is assumed to be uniform throughout the sample [54]. In the ultrathin film limit, the thickness of the film is less than the rf skin depth and the exchange length [17]. The skin depth is defined as

$$\delta = \frac{c}{\sqrt{2\pi\mu\omega\sigma}} \tag{2.1.34}$$

and the exchange length can be expressed as

$$d_{ex} = \frac{A}{\sqrt{2\pi M_s^2}} \tag{2.1.35}$$

[56]. Typical values of skin depth and exchange length for bulk bcc Fe (001) at room temperature are $\delta \sim 6 \times 10^{-5}cm$ and $d_{ex} = 3 \times 10^{-7}cm$ with the atomic planes of bcc Fe

(001) film being separated by a distance of $1.425 \times 10^{-8} cm$ [56] which satisfies the ultrathin film limit. In most practical ferromagnetic materials, the exchange length is usually in the range of 2-5 nm [11].

There are two main techniques which are used in the determination of the resonance frequency from the LLG equation of motion of the magnetization [17]. The first technique involves the solution of the coupled differential equations for the time-dependent magnetization components and the second technique involves the double derivatives $F_{\Psi\Psi}$, $F_{\Omega\Omega}$ of the anisotropic part of the magnetic free energy density, F. The second technique which involves the double derivatives of $F_{\Psi\Psi}$, $F_{\Omega\Omega}$ was developed by Smit and Beljers (1955) [17,57] with the resonance condition expressed as [17,57,59,58,54,116,130]

$$\omega = \frac{\gamma}{M sin\Psi}[F_{\Psi\Psi}F_{\Omega\Omega} - F_{\Psi\Omega}^2]^{\frac{1}{2}} \tag{2.1.36}$$

which is subjected to the equilibrium conditions of [59,17,54,116,130]

$$\frac{\partial F}{\partial \Psi} = 0 \tag{2.1.37}$$

and

$$\frac{\partial F}{\partial \Omega} = 0 \tag{2.1.38}$$

where Ψ and Ω are the magnetization angles and γ is the gyromagnetic ratio. These two equations, Eq.(2.1.37) and Eq.(2.1.38) clearly means that the ferromagnetic resonance frequency must be evaluated at equilibrium angles of Ψ and Ω of the magnetization, M (T,H) [17,54]. It can be observed from Eq.(2.1.36) that the resonance frequency is related to the second derivatives of the free energy, F and is essentially a measure of the "curvature" of the free energy, F or of the "stiffness" of magnetization.

In FMR spectrometers, two main parameters are usually measured [56]. These are the microwave power, P_m absorbed by the sample as a function of the applied dc magnetic field,

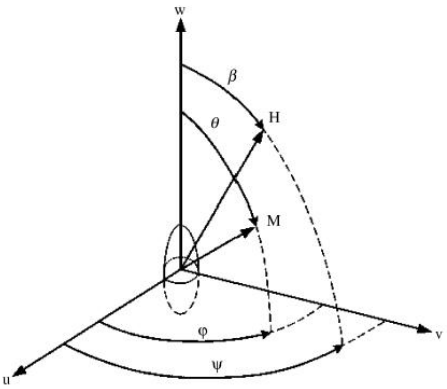

Figure 2.3: Geometry of magnetization and static field (H) in Smit-Beljers theory. Adopted from ref.[116]

H and the derivative of the absorption with respect to the field, H [56]. The microwave power, P_m which is absorbed by the sample is related to the component of the dynamic susceptibility in the direction of the microwave, h_o [56,60]. The susceptibility, χ can be expressed as [60,55]

$$\chi = \chi\prime - i\chi\prime\prime \tag{2.1.39}$$

The real part of the susceptibility, $\chi\prime$ is indicative of dispersive process and the imaginary part, $Im[\chi]$ is indicative of dissipation process [60,61]. For conductive samples, dissipation is mainly due to eddy currents and a non-zero imaginary susceptibility in ferromagnets can indicate an irreversible domain wall movement or an absorption due to a permanent moment [61]. The microwave power, P_m can be expressed as [60,56,17]

$$P_m = \frac{1}{2}\omega Im[\chi_y]h_o^2 \tag{2.1.40}$$

and this represents the energy which is transferred from the microwave to the sample[60]. The dissipation of this form of energy usually appears as heat as a result of the vibration of the lattice [60].

The magnetic susceptibility which is associated with the rf-magnetic field can be expressed

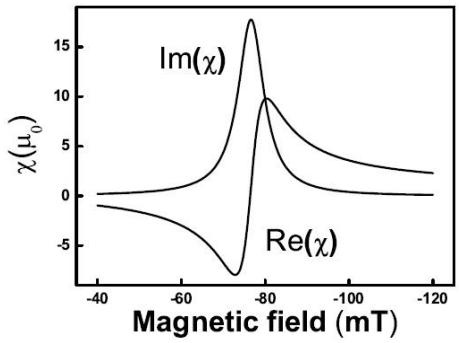

Figure 2.4: Real and imaginary parts of the longitudinal high frequency magnetic susceptibility as a function of an applied magnetic field. Adopted from ref.[126]

as [42,15]

$$\chi_{rf} = \frac{M_x}{H_{rf}} = \frac{\chi_H}{1 - \frac{\omega^2}{\omega_o^2}} \tag{2.1.41}$$

where $\chi_H = \frac{M_y}{H}$. The magnetic susceptibility, Eq.(2.1.41) has a maximum when $\omega = \omega_o$, where ω is the frequency of the rf-magnetic field and ω_o is the frequency of the magnetization precession [42,15]. Ferromagnetic resonance therefore occurs when $Im[\chi_y]$ is maximum and this corresponds to the maximum power which is absorbed by sample [56,42,17].

Since in an FMR experiment the microwave frequency, ω is fixed so that resonance can be achieved by sweeping the external dc field, H_o the resonance field, H_{FMR} can be expressed as the real part of [55,56,132]

$$\frac{\omega^2}{\gamma^2} = [H_{FMR} + 4\pi M_{eff} + \frac{K_1^{eff}}{2M_s}(3 + cos4\theta) + \frac{i\omega G}{\gamma^2 M_s}] \times [H_{FMR} + \frac{K_1^{eff}}{2M_s} cos4\theta + \frac{i\omega G}{\gamma^2 M_s}] \tag{2.1.42}$$

for the parallel configuration, where G is the Gilbert damping parameter and θ is the angle between the field and the crystal axis. In the case of perpendicular condition, the resonance condition can be expressed as [56,55,132]

$$\frac{\omega}{\gamma} = H_{FMR} - 4\pi M_{eff} + \frac{2K_1^{eff}}{M_s} \tag{2.1.43}$$

Equation(2.1.42) and (2.1.43) are only valid in high applied magnetic fields in which the dc magnetic moment is parallel to the external dc field, H_o [56,55].

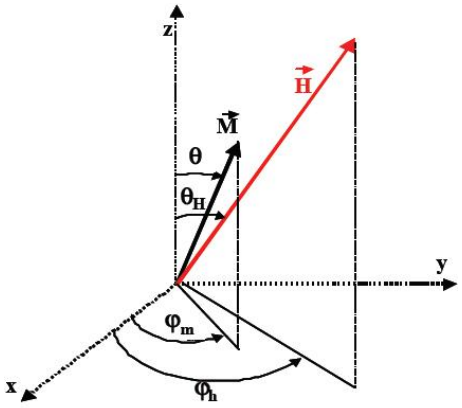

Figure 2.5: Spherical coordinates for the magnetization and magnetic field vectors used in the calculation of the ferromagnetic resonance frequency. Adopted from ref.[42]

For a thin magnetic film with an in-plane uniaxial anisotropy which is magnetized to saturation along the easy axis by a static external field, the Kittel FMR resonance can be written as [62]

$$\omega = \gamma\mu_o[(H_{ext} + H_k)(H_{ext} + H_k + M_s)]^{\frac{1}{2}} \tag{2.1.44}$$

If we ignore the saturation magnetization in Eq. (2.1.44) by setting the saturation magnetization, M_s to zero, we observe that Eq. (2.1.44) reduces to

$$\omega = \gamma\mu_o(H_{ext} + H_k) \tag{2.1.45}$$

Equation (2.1.45) is in agreement with [65,64] which is the experimentally observed frequency at lower modes [63]. When equation (2.1.44) is simplified and also by assuming a non-zero saturation magnetization, this result in the Kittel FMR resonance expression

$$\omega = \gamma\mu_o[H_{ext}^2 + H_k^2 + 2H_kH_{ext} + M_s(H_k + H_{ext})]^{\frac{1}{2}} \tag{2.1.46}$$

By assuming only second order terms in this expression, Eq.(2.1.46) reduces to

$$\omega = \gamma\mu_o(H_{ext}^2 + H_k^2)^{\frac{1}{2}} \tag{2.1.47}$$

which is also in agreement with the fact that resonances are quadratically positioned as a function of the applied field at higher modes [63].

There are certain factors which can affect the ferromagnetic resonance frequency. Some of these factors include, shape anisotropy and the magnetocrystalline anisotropy [11]. In the case of shape anisotropy this is so because different geometrical samples have different demagnetizing factor [11]. This effect means that the ferromagnetic resonance frequency condition for a sphere or a thin film whose field is either perpendicular to the plane or in plane might not be the same because each has different demagnetizing factor [11].

2.2 DAMPING IN ULTRATHIN MAGNETIC THIN FILMS

Phenomenologically, magnetic relaxation in metallic ferromagnetic films is expressed by the LLG equation, Eq.(2.1.32) [66]. The damping term is described by the second term on the right hand of Eq.(2.1.32). Clearly from Eq. (2.1.32), it can be observed that damping can occur when the magnetization in time dependent. The application of the LLG equation to a ferromagnetic thin film which is magnetized in plane or perpendicular to the plane leads to the prediction of the ferromagnetic resonance linewidth [67]. The ferromagnetic resonance linewidth, ΔH_{pp} is related to the magnetic damping parameter, α by [56,68]

$$\Delta H_{pp} = \frac{2}{\sqrt{3}}\alpha\frac{\omega}{\gamma} \tag{2.2.1}$$

where $\alpha = \frac{G}{\gamma M_s}$. The ferromagnetic resonance linewidth, ΔH_{pp} is proportional to the microwave frequency, ω and inversely proportional to the saturation magnetization, M_s. This is referred to as the intrinsic contribution to the linewidth [18]. However, it has been observed experimentally that there is an additional frequency independent contribution to the

linewidth and this is referred to as the inhomogeneous contribution [18]. This inhomogeneous contribution to the ferromagnetic resonance linewidth is as a result of disorder in the sample[18]. This disorder occurs as a result of two main processes [18]. Firstly, fluctuations in the magnetic properties of the material such as magnetization and secondly as a result of the fact that in a typical ferromagnetic resonance experiment, uniform precissional mode ($k = 0$) are excited and this then generate finite -k ($k \neq 0$) spin wave modes [18]. The homogeneous and inhomogeneous contribution to the ferromagnetic resonance linewidth is as a result of combined effect of the exchange interaction and the spin orbit coupling [68]. These two contributions to the ferromagnetic resonance linewidth are usually extracted from the relation [68,66,17,134,132,137]

$$\Delta H_{pp} = \Delta H_{inhomo} + \Delta H_{homo} = \Delta H_{inhomo} + \frac{2}{\sqrt{3}}\alpha\frac{\omega}{\gamma} \tag{2.2.2}$$

There are some mechanisms which can contribute to the ferromagnetic resonance linewidth. These are the intrinsic Gilbert damping, the broadening induced which occurs as a result of the magnetic inhomogeneity and the extrinsic magnetic relaxation [68].

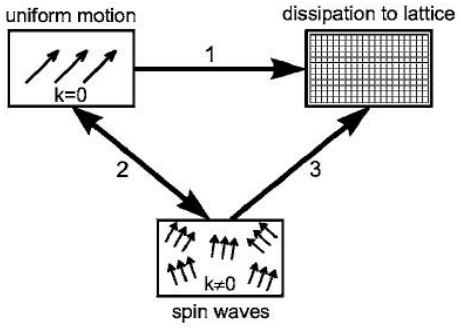

Figure 2.6: The uniform motion of the magnetization with $k = 0$ in an FMR experiment. Adopted from ref.[36,45]

In magnetic systems such as ultrathin films, the Gilbert damping torque describes the relaxation of the magnetization and the origin of the Gilbert damping in ultrathin films is

as a result of the spin-orbital coupling [47]. Experimentally, the Gilbert damping constant in thin magnetic films can be studied by measuring the peak-to-peak ferromagnetic resonance linewidth [68]. It has been established that, the Gilbert damping constant in ultrathin films is larger compared to their bulk counterpart due to the higher damping in strained films as compared to the relaxed films [68,69]. Typical example is Fe on semiconductor substrates in which the value of the dimensionless Gilbert damping constant, α is 4.1×10^{-3} for the thin films and 2.8×10^{-3} for the thick films [69].

2.3 LMSO

This section of the thesis work gives some brief introduction about LSMO, crystal structure, phase diagram, FMR of LSMO, some thin film techniques for fabricating LSMO and some potential applications of LSMO and the mixed valence manganites.

2.3.1 INTRODUCTION

The compounds which have attracted renewed attention are the manganite perovskites which have the form $T_{1-x}D_xMnO_3$ where T is a trivalent lanthanide cation (eg. La, Pr, Nd) and D is a divalent, eg. alkaline-earth (eg. Ca, Sr, Ba), cation [70,71,72]. The manganite perovskites have interesting properties and some of the properties are given below. The physical properties of the manganite perovskites, $T_{1-x}D_xMnO_3$ can be tuned by controlling the doping level, x [110]. The manganite perovskites are known to undergo phase transformation from the ferromagnetic metal to paramagnetic insulator and this phase transformation depends on the particular composition of the sample, internal stress, and the structural defects [90]. Due to this phase transformation in the manganite perovskites, an electron spin resonance (ESR) lines in the paramagnetic(PM) phase with large variations of the line parameters as a function of temperature, T has been observed [129]. The manganite perovskites have unusual electrical transport and magnetic properties [133]. This unusual

electrical transport and magnetic properties depends on factors such as doping level, the ratio of the Mn^{4+} to Mn^{3+} ions, and the interaction between the Mn^{4+}/Mn^{3+} and O^{2-} ions [101]. The electrical and magnetic properties of the manganite perovskites are related to the crystal structures as well as its microstructures [102]. Also, the interplay between the charge, spin and the orbital degrees of freedom give rise to magnetoelectronic phenomena in the manganite perovskites compounds [110]. One common feature which is exhibited by the mixed valence manganites is that their physical properties are closely related to their lattice constants and they have a strong dependence on hydrostatic pressure[123]. The mixed valence manganites exhibit other interesting properties such as high temperature superconductivity and ferroelectricity [123].

Research interest in the manganite perovskites was motivated by the need to develop insulating ferromagnet with high magnetization for high frequency applications and the discovery of high-temperature superconductivity in the cuprates [71,72]. Also, the observation of colossal magnetoresistance effect in the manganite perovskites added more interest to the research work [72,89,135]. By colossal magnetoresistance effect, it means that the electrical resistance of the these compounds changes as a result of the application of magnetic field [73]. Typical examples of the manganite perovskites include; $La_{1-x}Sr_xMnO_3$ (LSMO), $La_{1-x}Ca_xMnO_3$ (LCMO) and $La_{1-x}Ba_xMnO_3$ (LBMO).

The end members of the manganite perovskites, thus $LaMnO_3$ and $CaMnO_3$ are antiferromagnetic and insulating but doping at $x \approx \frac{1}{3}$ yields a ferromagnetic and conducting material [71,74]. Typical examples include; $La_{0.7}Ca_{0.3}MnO_3$(LCMO) which has a Curie temperature, $T_c = 220K$ and a low temperature resistivity, $\rho_o = 10^{-5}\Omega m$ and $La_{0.7}Ba_{0.3}MnO_3$(LBMO) which has a Curie temperature, $T_c = 310K$[75,71]. For the perovskite $LaMnO_3$ which is an insulating layered antiferromagnetic with a Néel temperature, $T_N = 150K$, by replacing La^{3+} with a divalent cation (eg. Ba,Ca or Sr), the mixed

compound $La_{1-x}Sr_xMnO_3$ becomes ferromagnetic and conducting at room temperature at $x \approx 0.3$ [71,11].

The most researched of the manganite perovskites currently, is the alkaline-earth-substituted lanthanum manganites, and a typical example is $La_{1-x}Sr_xMnO_3$ (LSMO). LSMO has special properties such as high electrical conductivities, a high Curie temperature of 370K which is above room temperature at $x \approx \frac{1}{3}$ [77,78,72,11,154] and the presence of superstructures at $x = \frac{1}{8}$ and $x = \frac{1}{2}$ [71]. In a situation where the strontium (Sr) concentration is $\frac{1}{8}$, $(x = \frac{1}{8})$ various superstructure and characteristic temperatures have been observed. A ferromagnetic state(FM) has been observed below $T_c = 180K$, metallic down to $T_c = 150K$ and insulating below $T_c = 150K$ [141]. Also, around $T_{JT} = 280K$ the phenomenon of Jahn-Teller transition has been observed from Ó to O phase and above $T_R = 475K$, the rhombohedral ($R\bar{3}C$) R phase has also been observed [141]. Figure 2.7 shows the thermal expansion vrs temperature of a single crystal $La_{\frac{7}{8}}Sr_{\frac{1}{8}}MnO_3$ which can be used to explained such a phenomenon.

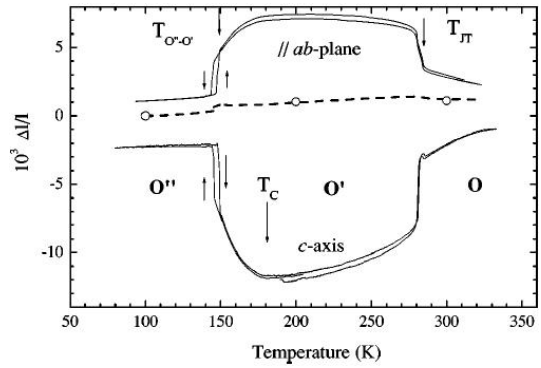

Figure 2.7: Schematic diagram of thermal expansion vrs temperature of $La_{\frac{7}{8}}Sr_{\frac{1}{8}}MnO_3$ single crystal. Adopted from ref.[141]

Thin films of $La_{1-x}Sr_xMnO_3$(LSMO) have fascinating magnetic and electric properties[79].

The electronic properties of LSMO are usually described by the band theory as nearly half-metallic [80]. By half-metallic it means that LSMO has one spin-up or spin-down electron states in its Fermi level [79,80]. Among the manganite perovskites, $La_{0.7}Sr_{0.3}MnO_3$ is one of the most studied compounds and has special properties including; high conductivity at room temperature, fully spin -polarized conduction band, high stability of the crystal structure under certain oxygen pressures and also the ability to behave as a p-type semiconductor at room temperature [81,99,136].

2.3.2 CRYSTAL STRUCTURE

$La_{1-x}Sr_xMnO_3$(LSMO) belongs to the ABO_3 perovskite oxide family. The ideal cubic perovskite structure of ABO_3 is indicated in figure 2.8 with a lattice constant of 0.388 nm [71,82,72]. In figure 2.8, the larger rare earth ions (eg. La, Ca) is similar in size to O^{2-} and it occupies the 12 coordinated A-site and the transition metal ions (eg. Mn) occupy the octahedral B-sites [71,98,72].

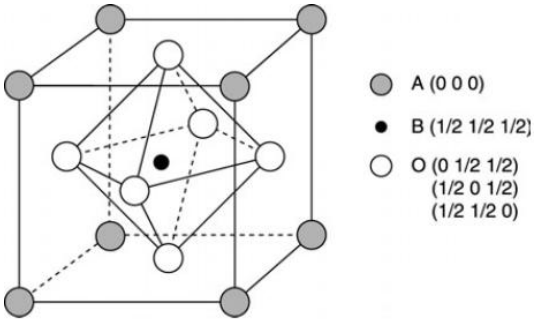

Figure 2.8: The ideal cubic perovskites, ABO_3. A is a large cation similar in size to O^{2-}, B is a small cation such as Mn^{3+} or Mn^{4+}, octahedrally-coordinated by oxygen. Adopted from ref.[71,72]

LSMO has two types of crystal structures and this depends on the temperature, oxygen pressure and the chemical composition [77]. These crystal structures are the rhombohedral

(R$\bar{3}$C) and the orthorhombic (Rbnm) and these structures have distorted vertex-sharing of MnO_6 octahedral [77]. Typical crystal structures of LSMO are shown in figure 2.9 and figure 2.10

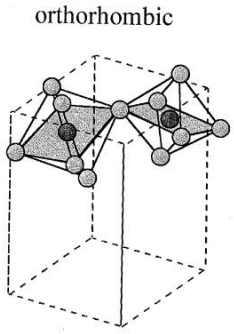

Figure 2.9: Schematic drawing of the arrangement of MnO_6 octahedral in orthorhombic LSMO lattice where the dashed lines corresponds to the unit cell of each lattice. Adopted from ref.[77]

The end members of the manganite perovskite; $CaMnO_3$ and $LaMnO_3$ have Pbnm D_{2h}^{16} with $Z = 4$ orthorhombic structure at room temperature [83,82,72,71]. At a temperature $T \approx 600^oC$, $LaMnO_3$ shows an orthorhombic or rhomboherdal crystallographic transformation and this transformation is attributed to the oxidation of Mn^{3+} to Mn^{4+} ions [82]. The crystal structure of $La_{0.7}Sr_{0.3}MnO_3$ is rhombohedral with (R$\bar{3}$C) D_{3d}^6 with $Z = 2$ space group [83]. A typical Pbnm orthorhombic $RMnO_3$ compound is structurally distorted with respect to the cubic perovskite [83]. These distortions which occurs with respect to the cubic perovskite is as a result of the rotation of the oxygen octahedra and the lanthanum ion shifts like in the orthoferrite crystals and the Janh-Teller effect of the oxygen octahedra of the e-type[139].

Generally, the structure of the manganite perovskites is governed by the tolerance factor, t which is related to the ionic radii of the constituents atoms. This tolerance factor according

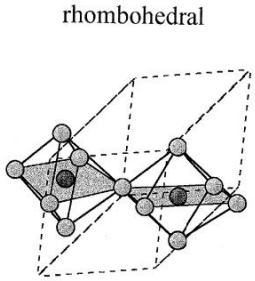

Figure 2.10: Schematic drawing of the arrangement of MnO_6 octahedral in rhombohedral LSMO lattice where the dashed lines corresponds to the unit cell of each lattice. Adopted from ref.[77]

to Goldschmidt can be expressed as [71,72,11]

$$t = \frac{(r_A + r_o)}{\sqrt{2}(r_B + r_o)} \tag{2.3.1}$$

For an ideally sized ions, $t = 1$ and for the perovskite structure, $0.89 < t < 1.02$ is indicative of a stable structure [71,72,11]. $La_{0.7}Sr_{0.3}MnO_3$ which has special properties inculding spin-polarized conduction and higher conductivity at room temperature [81,99] has a crystal structure as in figure 2.11

2.3.3 PHASE DIAGRAM OF LSMO

Lanthanum-strontium manganites, $La_{1-x}Sr_xMnO_3$ (LSMO) materials display an enormously rich phase diagram by varying the temperature and the doping level, x with phases showing behaviors as interesting as colossal magnetoresistance [71,72]. For instance at $x \approx \frac{1}{3}$, the material behaves as a ferromagnetic half metal, that is, with the Fermi level within a gap in the minority-spin density of states [71,11,80]. The rich phase diagram of LSMO which is sometimes considered as complex with various magnetic phases which may either be conductive or insulative can be attributed to the competition between the charge,

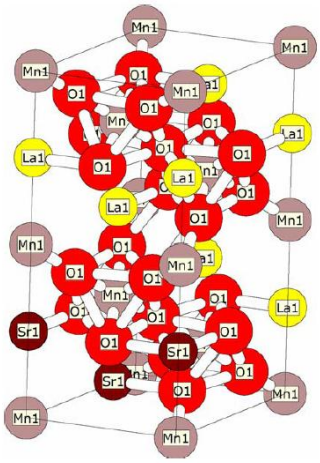

Figure 2.11: Crystal structure of one of the most studied manganite perovskites, $La_{0.7}Sr_{0.3}MnO_3$. Adopted from ref.[82]

spin, orbital and the lattice [112,113]. There is a deep connection between the conductivity and ferromagnetism and this can be expressed as [71]

$$\sigma_c = (\frac{xe^2}{rh})(\frac{T_c}{T}) \tag{2.3.2}$$

where x is the doping and r is the Mn-Mn distance. This relation, Eq. 2.3.2 is only valid in the limited range of $0.2 < x < 0.4$ [71].

The existence of the ferromagnetic(FM) phase and the antiferomagnetic (AF) phases which appears on the phase diagram is partly due to the coexistence of the AF superexchange interactions [110]. The AF superexchange interaction is the type of interaction between the t_{2g} spins and the electronic anisotropy which arises from the orbital ordering of the conduction e_g electrons [110].

Konishi et. al (1999) studied the magnetic and transport properties of LSMO thin films which were thinner than the coherence epitaxy, ζ. The LSMO thin films which were studied were deposited on three different substrates and they observed a phase diagram which

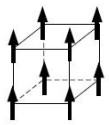

Figure 2.12: A schematic illustration of the magnetic structure in a FM magnetic state. Adopted from ref.[115]

consisted of a ferromagnetic metal, A-type and C-type ferromagnetic insulators (AFI), in the x against the c-axis/a-axis ratio plane [114]. Tandeloo et. al (2000) used the method of neutron diffraction for an intensive research on LSMO and they observed two different orthorhombic phases and one rhombohedral crystal structure [111]. A typical magnetic structure in a FM state is shown in figure 2.12 above.

Typical phase diagram of $La_{1-x}Sr_xMnO_3$ (LSMO) is as shown in figure 2.13. In figure 2.13, it can be observed that LSMO is insulating up to about $x = 0.15$ (FI) whiles metallic at $x > 0.15$ (FM). It can also be observed from figure 2.13, that LSMO shows an insulating canted AF structure(CI) at doping level $0 \leq x < 0.1$ [72].

2.3.4 FERROMAGNETIC RESONANCE OF LSMO

Ferromagnetic resonance(FMR) which is one of the most powerful experimental technique as a result of the its high resolution and high sensitivity can be used for the study of metallic systems such as ultrathin metallic films (eg. LSMO) [90,54,124]. Ferromagnetic resonance which can be described as the motion of the magnetization in an external magnetic field can be expressed by the Landau-Lifshitz-Gilbert (LLG) equation, Eq.(2.1.32) with the FMR

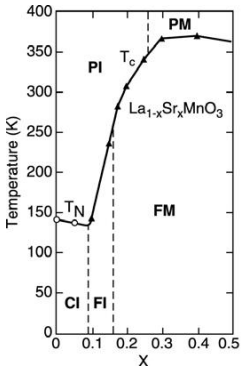

Figure 2.13: Phase diagram showing transition temperature versus concentration, x of single crystals of $La_{1-x}Sr_xMnO_3$. Adopted from ref.[72]

linewidth given by Eq. (2.2.2) [124,68].

In thin magnetic films such as LSMO, the anisotropic energy can be expressed as Eq. (2.1.2) and by taking the first two terms of Eq. (2.1.2) , the frequency at which resonance occurs can be expressed as [90]

$$(\frac{\omega}{\gamma})^2 = [Hcos(\psi-\eta) - H_{eff}cos^2\psi + \frac{2K_2}{M}] \times [Hcos(\psi-\eta) - H_{eff}cos2\psi + \frac{K_2}{M}(1+cos^2 2\psi)] \tag{2.3.3}$$

where H_{eff} is the effective field which is expressed as [90]

$$H_{eff} = 4\pi M - \frac{2K_1}{M} \tag{2.3.4}$$

and η is the angle between the external magnetic field and direction z normal to the film and ψ is the angle between the magnetization, M and the main axis. The angle ψ can be determined from the equilibrium condition [90] as

$$Hsin(\psi-\eta) - \frac{1}{2}(H_{eff} - \frac{2K_2}{M}sin2\psi) - \frac{2K_2}{M}sin2\psi sin^2\psi = 0 \tag{2.3.5}$$

In an FMR experiment in ultrathin magnetic films such as LSMO, the magnetic anisotropy of the film can be determined by analyzing the angular variation of the field, H_{res} [122]. The

behaviour of the angular variation of the field, H_{res} at different fields shows sinusoidal-like shape [122]. Typical FMR spectra measurement for different orientations for a bicrystalline $La_{0.75}Sr_{0.25}MnO_3$ films at temperature of 125K indicating this sinusoidal-like shape is indicated in figure 2.14

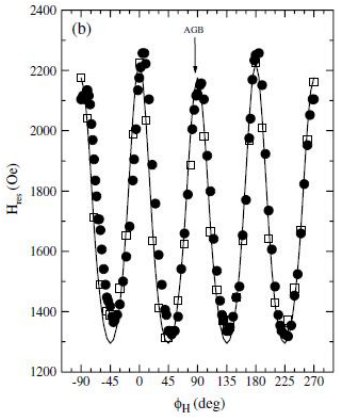

Figure 2.14: The angular variation of the magnetic field, H_{res} of a bicrystalline $La_{0.75}Sr_{0.25}MnO_3$ film at a temperature of 125K. Adopted from ref.[122]

2.3.5 SOME TECHNIQUES OF FABRICATING LSMO AND MANGANITE THIN FILMS

There are several techniques which are used for fabricating thin films. Some of these thin films fabrication techniques include; sol-gel dip coating, molecular beam epitaxy (MBE), pulsed laser deposition (PLD), metal organic chemical vapour deposition (MOCVP) and spray pyroysis. But the pulsed laser deposition technique from sintered ceramic target have mainly been used for the growth of the manganites thin films [71]. For pulsed laser deposition technique, critical factors such as the atmosphere in the chamber and the temperature of the substrate are very critical for the growth of high quality thin films [71]. For example, by using an oxygen pressure of $10-50Pa$ and a substrate of MgO, $SrTiO_3$ (STO) or $LaAlO_3$ (LAO) which has been heated to about $600-800^oC$, good quality films have been grown

[71]. This technique has been used to grow quality thin films such as $La_{0.7}Sr_{0.3}MnO_3$, $La_{0.67}Bd_{0.33}MnO_3$ and $La_{0.7}Ca_{0.3}MnO_3$[71]. The pulsed laser deposition technique can be used in growing thin films of the order 100nm or less but the molecular beam epitaxy technique is mainly used to grow highest quality films [71,84,11]. One of the disadvantages of the pulsed laser deposition technique is the tendency for the micrometer-size droplets which is ejected from the target to litter the growing film [11]. This barrier can be overcome by working at an energy density which is close to the ablation threshold by using a fully dense targets [11]. The ablation threshold which is a material and wavelength dependent property is defined as the minimum fluence in which the expulsion of a given material in the form of hot plasma is obtained[138]. Although the pulsed laser deposition technique is used in growing quality thin films, the magnetron sputtering technique is more preferable than the PLD technique as a result of its compatibility with current existing large scale integrating (LSI) processes [87].

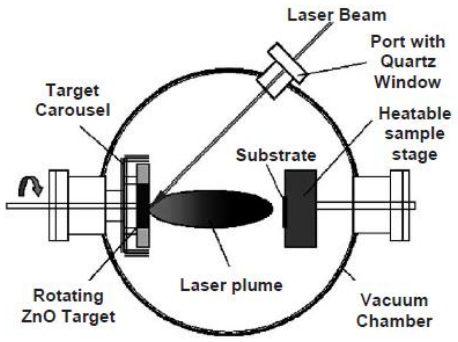

Figure 2.15: A schematic diagram of the pulsed laser deposition (PLD) experimental setup. Adopted from ref.[117]

In molecular beam epitaxy, the pressure of the evaporating species is usually in the range

of $10^{-6} - 10^{-4}Pa$. During the molecular beam epitaxy process in the fabrication of thin films, sometimes the atoms from the evaporation source are scattered before they get to the substrate [11]. In order to overcome this barrier, the mean free path of the emitted atoms from the evaporation source must be greater than the size of the chamber. The mean free path is expressed as $\frac{6}{P}$, where P is the pressure [11]. The technique of electrochemistry can also be used in growing thin films of the manganites. During this process, $LaMnO_3$ is deposited unto $SrTiO_3$ substrate from a 1M solution of lanthanum and manganese nitrate under ultraviolet illumination [71].

There are several oxide materials with perovskite structure which can be used as substrate for high epitaxial growth of LSMO thin films but $SrTiO_3$ (STO) and $LaAlO_3$ (LAO) substrates are mainly used for growing quality films as a result of the small misfits which emerges after the fabrication process [86,91]. This is because the lattice constant of STO, $a_{STO} = 0.391nm$ and LAO, $a_{LAO} = 0.380nm$ are comparable to the lattice constant of LSMO, $a_{LSMO} = 0.388nm$ at room temperature [71,91]. In the case of LSMO thin film which is fabricated on STO substrate, one can observe a misfit strain, $\varepsilon_m = 0.007732$ at room temperature [79]. This misfit strain is smaller as compared to the misfit strain, $\varepsilon_m = 0.0079$ at a temperature of 800^oC [79]. The misfit strain was calculated using the expression [79]

$$\varepsilon_m = \frac{(a_{STO} - a_{LSMO})}{a_{LSMO}} \tag{2.3.6}$$

Furthermore, STO has a thermal expansion coefficient ($\approx 11 \times 10^{-6}K^{-1}$) which is close that of LSMO ($\approx 11.5 \times 10^{-6}K^{-1}$) and this guarantees a crystal misfit of less than 1 percent for all temperatures below 1000K [79]. For LSMO thin film which is fabricated on LAO substrate, an in-plane compressive strain of -0.021 can be observed. The in-plane compressive strain was calculated using the relation[119]

$$\varepsilon_c = \frac{a_{LAO} - a_{LSMO}}{a_{LAO}} \tag{2.3.7}$$

Some of the other substrates which can be used in fabricating LSMO thin films using the technique of pulsed laser deposition are ZnO, MgO, $NdGaO_3$, $LaGaO_3$ (LGO) and Al_2O_3 (AO)[81,90,87,121,127,149]. It can be observed from the above that most of the LMSO thin films are deposited onto oxide substrates by pulsed laser deposition technique[87]. This is done so that the effect of lattice mismatch can be minimized [91]. In order to achieve good quality colossal mangnetoresistant manganites(CMR) thin films such as LSMO, there are other two materials properties of CMR film and the substrate that are very critical apart from lattice mismatch [91]. These are chemical reaction and different thermal expansion [91]. The difference in the thermal expansion coefficients between the thin films of the oxide and the substrate results in a structural phase transformations [91].

The presence of strain in fabricated LSMO thin films can be attributed to the difference in crystal structure between the film and the substrate [79,120]. It has been established that thin film properties of the manganite perovskites such as LSMO, LCMO and LBMO are not only affected by lattice misfits but also by annealing conditions, layer thickness, and mechanism of strain relaxation[88]. It has also been established recently that by depositing Au on top of a 4 nm thick LSMO film results in a drastic reduction in the Curie temperature to 188 K with respect to an uncoated LSMO thin films of the same thickness [100]. Also, recently studies have shown that the magnetic and transport properties of the thin films of the CMR materials can be improved by postannealing in oxygen. This improvement in the magnetic and transport properties can be attributed to the oxygen incorporation which transforms Mn^{3+} ions to Mn^{4+} with smaller ionic radii which induces the changes in the unit-cell volume [101]. Research work on the effect of tensile strain on LSMO thin films have also shown a reduction in the Curie temperature and this anomaly was successfully explained using the idea of double exchange interaction [103]. The double exchange which was proposed by Zener [129] explains this reduction in the Curie temperature as a result of the increase of the in-plane Mn-O bond length which results in the decrease of the hopping

term between the $Mn^{3+} - Mn^{4+}$ ion [103].

The double exchange interaction in the colossal magnetoresistance (CMR) perovskites is as a result of the the ferromagnetic(FM) interactions in the Mn ions [129]. Due to the coupling between the Mn ions, the double exchange interaction model give rise to a magnetic susceptibility that can be described by the isotropic Heisenberg-like interaction between the $Mn^{3+} - Mn^{4+}$ pairs. The Heisenberg-like model can be expressed as [129]

$$H = -2J \sum_{<i,j>} S_1^i . S_2^j + g\mu_B \sum_{(i,j)} (S_1^i + S_2^j).H \tag{2.3.8}$$

where S_1 and S_2 are the spins of Mn^{4+} and Mn^{3+} species respectively, with $S_1 = \frac{3}{2}$ and $S_2 = 2$, H is the external magnetic field, and $< i, j >$ runs over all possible $Mn^{3+} - Mn^{4+}$ pairs [129].

2.4 SOME POTENTIAL APPLICATIONS OF LSMO AND THE MIXED VALENCE MANGANITES

The potential applications of the mixed valence manganites are based on its physical and chemical properties. Typical physical property is the temperature dependence of the resistivity and the magnetoresistance [71]. Thin films of the manganite perovskite with ferromagnetic colossal magnetoresistance are potential candidates for tunable microwave filters [93]. This process can be achieved when thin films of the manganite perovskite are stacked on high temperature superconducting YBCO thin films [93]. It has been established that microwave tunability has already been achieved by using ferromagnetic $La_{0.67}Sr_{0.33}MnO_3$ and other thin films materials such as tunable barium strontium titanate paraelectric films [94]. On the research front also, the manganite perovskites can be used to fabricate multilayers and also to investigate the magnetic interactions at the interfaces of other materials due to the fact that the magnetic states of these manganite perovskites can easily be controlled by changing the carrier doping and temperature [92]. The presence of the unusual

electrical and magnetic properties of the colossal magnetoresistance in the manganites perovskites have been considered for application including ferroelectric field effect transistor (FeFET), infrared (IR) bolometric devices, spin tunnel junctions, microwave active components, infrared optical sensors, photonic devices, magnetoelectronics, spin sensitive devices and high-density memory application [95,91,96,89,90,85,89,75,99].

Among the colossal magnetoresistance materials, $La_{0.7}Sr_{0.3}MnO_3$ has the highest Curie temperature and this makes it very promising for room temperature applications [95,99]. In spintronics technology, $La_{0.67}Sr_{0.33}MnO_3$(LSMO) is considered as the favourite candidate as a result of the half-metallicity [85,78]. The presence of half-metallicity allows for very high spin polarization and this yields high tunnel magnetoresistance (TMR) values according to the Julliere equation. The Julliere equation can be expressed as [97]

$$TMR = \frac{P_1 P_2}{1 - P_1 P_2} \tag{2.4.1}$$

where P_1 and P_2 shows the polarisation of top and bottom ferromagnetic layers. The prediction of nearly 100 percent spin polarisation in $La_{\frac{2}{3}}A_{\frac{1}{3}}MnO_3$ where $(A = Ca, Sr, Ba)$ atoms further boost the idea of 1850 percent TMR- ratio for $La_{\frac{2}{3}}Sr_{\frac{1}{3}}MnO_3/SrTiO_3/La_{\frac{2}{3}}Sr_{\frac{1}{3}}MnO_3$ magnetic tunnel junctions at 4K [76,97,80,149]. Tunnel magnetoresistance (TMR) has potential applications including magnetic field sensors or non-volatile magnetic random access memories [97].

In the area of the magnetoresistance applications of the manganite perovskites, $La_{1-x}A_xMnO_3$ where A is a divalent element such as Sr, Ca, Ba, due to the considerable changes in the resistance in strong fields at 1T, practical applications have considerably been restricted [125]. Progress in this area has been achieved through the use of fine-crystalline manganites as well as samples including microscale defects or spin-disordered areas where higher magnetoresistivity has been observed for the fine-crystalline manganites than their single crystal counterpart at low temperatures [125].

The alkaline-earth-substituted lanthanum manganites, such as $La_{1-x}Sr_xMnO_3$(LSMO) has potential applications including anode and interconnector materials for solid-oxide cells [77]. It has been anticipated that a manganite/superconductor layer structures could be useful for ultrasonic wave amplification, thermal switching and thermocouple infrared detection [71].

The manganite perovskites have intrinsic magnetocaloric effect which makes it an interesting material for magnetic refrigeration such as the Ericsson-cycle magnetic refrigerator which has a wide working span [71,107,106]. Magnetic refrigeration which is based on the idea of magnetocaloric effect(MCE) is a viable and competitive cooling technology which has potential advantage of environmental friendliness than the gas refrigeration [107]. By magnetocaloric effect it means that an application or removing of magnetic field to the manganite perovskites results in an isothermal entropy change, ΔS and adiabatic change in temperature ΔT_{ad} [108,109]. It has been established that magnetic cooling which is based on MCE is a promising alternative technology to the classical refrigeration such as air conditioning and liquefaction of gases [109]. In the chemical industries also, some of the potential applications of the manganites include catalysis, such as catalysts for automobile exhausts, oxygen sensors and solid electrolytes [71].

There are several reasons why currently it has been difficult for commercial devices based on LSMO to be achieved especially in the area of semiconductor technology. Some of the reasons include, large lattice mismatch between the CMR manganites films and the semiconductor substrate (eg. Si) [91]. Typical values include, the CMR manganite which has a lattice parameter $a = (3.8 - 3.9) \times 10^{-10}m$ and the semiconductor substrate has a lattice parameter $a = 5.431 \times 10^{-10}m$ for Si and $a = 5.653 \times 10^{-10}m$ for GaAs [91]. Also, the large difference in thermal expansion coefficient between the CMR thin films and the substrate and the severe chemical reaction between the substrate (eg. Si) and the deposited

film layer have also contributed to this problem [104]. The thermal expansion coefficient for a typical CMR material such as LSMO at room temperature is $11.5 \times 10^{-6} K^{-1}$ whiles the thermal expansion coefficient for the single crystalline Si substrate at room temperature is $9 \times 10^{-8} K^{-1}$ [105].

Chapter 3

EXPERIMENTAL METHOD

3.1 INTRODUCTION

Conventionally, in the experimental determination of the ferromagnetic resonance of a magnetic sample, measurements are usually carried out using a resonator and a waveguide but recent studies in the area of microfabrication techniques have also shown that FMR measurements in the case of small-sized samples over a wide frequency range can also be achieved using the coplanar waveguide (CPW) technique [144,18,145]. These above mentioned techniques for FMR determination ensure that a high frequency magnetic field is concentrated onto a remarkably narrow signal line [144]. The shorted waveguide technique can also be used experimentally in the determination of the FMR especially the angle dependence of ferromagnetic resonance linewidth and two magnon losses [146] but in the case of this work, the EPR spectrometer was used in the determination of the FMR. In all the above mentioned techniques of determining FMR experimentally, the coplanar waveguide (CPW) technique provides one of the best means to perform a large angle ferromagnetic resonance as a result of the fact that the power which is coupled to the device is most effective than the usual conventional cavity or the hollow waveguide technique[147]. When the coplanar waveguide technique is to be used to determine the FMR, a static magnetic field can be applied parallel to the magnetic sample and the FMR signals are measured using a vector

network analyzer (VNA) [144]. In the next section of the experimental method, a summary of issues concerning the LSMO samples and basics of the EPR spectrometer and the experimental procedure are discussed.

3.1.1 LSMO SAMPLES AND BASICS OF THE EPR SPECTROMETER

LSMO thin film of different unit cells were grown using the pulsed laser deposition technique on (001) $SrTiO_3$(STO) substrate. The thin films were cut into smaller dimensions of $1 \times 1mm^2$ pieces. This was done in order to keep a resonance value of the quality factor. The quality factor, Q is related to the sensitivity of the EPR spectrometer. As the quality factor is increased, the sensitivity of the EPR spectrometer also increases. The microwave cavity which is characterized by the quality factor Q, indicates how efficiently the cavity of the EPR spectrometer stores the microwave energy. The quality factor, Q can be expressed as

$$Q = \frac{2\pi(E_s)}{E_d} \tag{3.1.1}$$

where E_s is the energy stored and E_d is the energy dissipated per cycle. The energy which is dissipated per cycle is the amount of energy which is lost during the microwave period.

FMR measurements were carried out with a Bruker Elexsys E 500 EPR spectrometer using an X-band frequency of 9.75GHz microwave source and a TE_{102} model cavity. In this spectrometer, the applied dc magnetic field was in the horizontal plane and the microwave magnetic field was vertical. A block diagram of the Bruker Elexsys E 500 EPR spectrometer system is shown in figure 3.1. A personal computer was used as a system controller and for data acquisition. In figure 3.1, the microwave bridge houses the microwave source and the detector and then the magnet which generates the required dc magnetic field which is needed for the experiment.

The block diagram of the microwave bridge is shown in figure 3.2. The microwave frequency

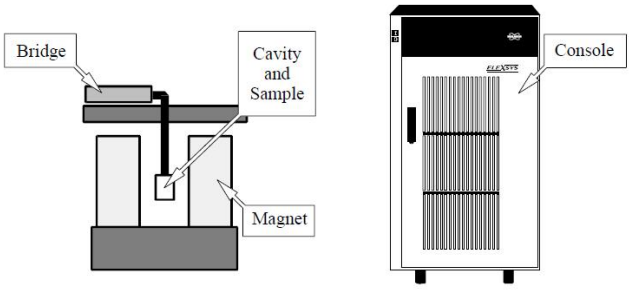

Figure 3.1: A schematic block diagram of an EPR spectrometer. Adopted from ref.[148]

of the microwave resonance cavity of the Elexsys E 500 spectrometer is fixed to an eigen frequency of the cavity and the magnetic field is increased until resonance absorption of the spin system occurs. In the ideal case, the cavity stores all the microwave energy at eigen-resonance (resonance). In figure 3.2, the microwave power from the source, A is reflected from the cavity and is detected at the diode.

3.1.2 EXPERIMENTAL PROCEDURE

FMR measurement was carried out on the 15uc thick LSMO thin film. This was done by positioning the 15uc thick LSMO thin film in a particular orientation (eg.[001]) in the sample holder made of glass. The sample holder which contains the LSMO thin film was inserted in the cavity of the Elexsys E 500 spectrometer for angular dependence of FMR spectrum to be recorded on the computer. This was achieved by rotating the sample holder which contains the LSMO thin film with a goniometer which was mounted on top of the cavity of the Bruker Elexsys E 500 spectrometer. The applied dc magnetic field was swept through the LSMO sample in the cavity till ferromagnetic resonance is achieved. At ferromagnetic resonance, the power which was absorbed by the LSMO thin film is a maximum. The FMR spectrum was recorded on the Bruker Elexsys E 500 spectrometer at a frequency of 9.75GHz, with a power of 0.6325mW, tolerance of 1.00K, modulation

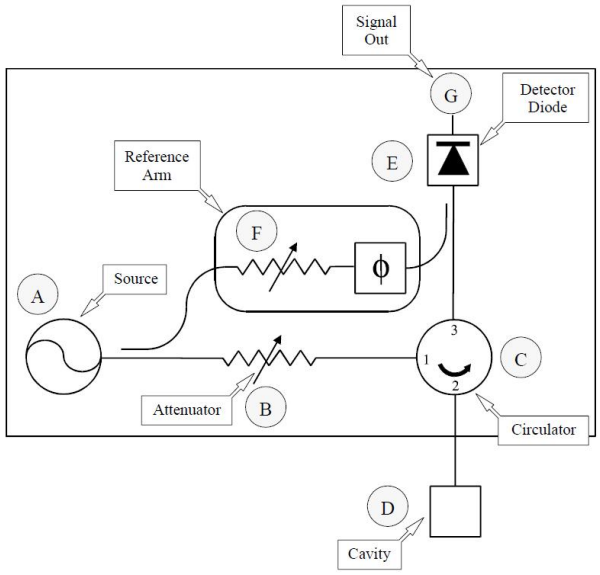

Figure 3.2: A block diagram of a microwave bridge. Adopted from ref.[148]

frequency of 100.00kHz, modulation amplitude of 10.00 and power attenuation of 25.0dB. In order to avoid contaminating the microwave cavity of the spectrometer with paramagnetic contaminants which produces spurious EPR signals, the sample tube was consistently wiped with a tissue paper.

Angular dependence of FMR spectra were recorded with the magnetic field rotated in the film plane (in-plane geometry) or in the plane which is perpendicular to film plane (out -of-plane geometry). It should be noted that due to restrictions of the experimental setup in the in-plane geometry, the microwave magnetic field is perpendicular to the film whiles in the case of the out-of-plane geometry, this field is in the plane of the film. The coordinate system which was used for the measurement and analysis of the out-of-plane dependence is as shown in figure 3.3. The goniometer was used to carry out the measurement of the out-of-plane dependence of the FMR. The data obtained from the experiment were then

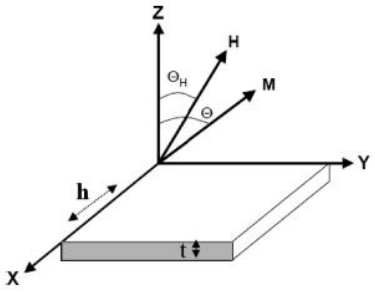

Figure 3.3: The coordinate system which was used for the measurement and analysis of the out-of-plane angular dependence of FMR. Adopted from ref.[131]

analyzed using Matlab.

Chapter 4

RESULTS AND DISCUSSIONS

The ferromagnetic resonance (FMR) spectrum at $T = 150K$ observed for the 15uc thick LSMO thin film which was deposited on STO substrate is illustrated in figure 4.1. The coordinate system which was used for the measurement of the FMR spectrum is shown in figure 3.3. As shown in figure 4.1, the spectrum clearly evolves as the resonance field, H_{res} is rotated in-plane. The spectrum in figure 4.1 is sinusoidal-like in nature which is in agreement with ref.[122]. That is, the angular variation of the resonance field, H_{res} presents a sinusoidal-like shape. In figure 4.1, it can be observed that there is a critical orientation for only a single uniform FMR mode. This single uniform FMR mode according to Puszkarski(1970) is attributed to the fact that at surfaces of a ferromagnetic film such as LSMO, there exists surface anisotropy which allows the excitation of an exchange-dominated non-propagating surface mode [143].

The resonance widths of the 15uc thick LSMO thin film such as in figure 4.1, is as a result of the homogeneous and inhomogeneous contributions [90]. The homogeneous contribution to the resonance width depends on factors such as microwave frequency and saturation magnetization [18]. The inhomogeneous contribution to the width of the FMR spectrum such as in figure 4.1 can be related to the variation of the magnetization, demagnetization parameters, anisotropy field and damping parameters in the LSMO thin film sample[90].

The significance of the resonance width in the LSMO sample is that it can give some information on the spin-lattice relaxation in the magnetic sample[2]. Also, another significance to the width of the resonance line in the 15uc thick LSMO sample is that it can be used to characterize the contribution of the intrinsic loss mechanisms and the determination of the magnetic inhomogeneities in the LSMO thin film [55].

The maxima and minima with negative and positive curvature (as depicted in figure 4.1) would either increase or decrease the resonance field respectively, and this depends on the magnetization direction [130]. The maxima and minima of the resonance spectrum in figure 4.1, are as a result of the singled-valued double differentiable function in the resonance condition of Eq. (2.1.36)[130]. The resonance position of the FMR spectrum in figure 4.1, is indicative of in-plane anisotropy. The in-plane anisotropy in the LSMO thin film can occur when an oriented or an epitaxial film of the magnetic material is grown with its easy axis perpendicular to the film plane[11]. Usually, in LSMO, the easy axis is aligned with the maximum tensile strain direction [154]. According to Boschker et. al (2010) they observed that an LSMO which was fabricated on STO (110) substrate, the tilt of the [110] vector was in the [001] direction favours a partially out-of-plane axis. The occurrence of the component of the easy axis results in magnetic domain formation which is due to the high demagnetization energy of the LSMO thin film in the out-of-plane direction [154].

The main feature of the FMR spectrum of the 15uc thick LSMO sample in figure 4.1 is broad which is basically single FMR line. This is also in agreement with FMR results on $(La, Sr)MnO_3$ bicrystalline films which were deposited on STO substrate [122]. The FMR spectrum of the 15uc thick LSMO sample has a maximum for orientation angles; 15^o, 46^o, 104^o and 151^o and the minimum of the FMR spectrum occurs at 28^o, 77^o, 118^o and 167^o. The mean maximum of the resonance field was 1229.5 Oe and the mean minimum of the resonance field was 910.875 Oe. The mean maximum and minimum of the resonance fields

were obtained by taking the mean of maximum of the four maxima from the amplitude of the sinusoidal-like shape and the mean minimum was also obtained by taking the mean of the minima of the amplitude of the sinusoidal-like shape or the ferromagnetic spectrum. From the mean maximum and mean minimum of the resonance field, this results in a center position of 1070.1875 Oe and the width which is sometimes approximated as the full width half maximum (FWHM) of 159.3125 Oe. As can be observed in figure 4.1, the amplitude of the FMR spectrum are unequal and this might be attributed to the existence of a uniaxial anisotropy [122]. This uniaxial or planar anisotropy which might have occurred during the growth of the 15uc LSMO thin film is due to the film substrate thermal expansion mismatch, lattice mismatch or the film microstructure[146]. According to Celinski et.al (1997) [56], the angular dependence of the resonance field, H_{res} yields K_1^{eff}. The surface plot of the 15uc thick LSMO thin film at $T = 150K$ as shown in 4.2.

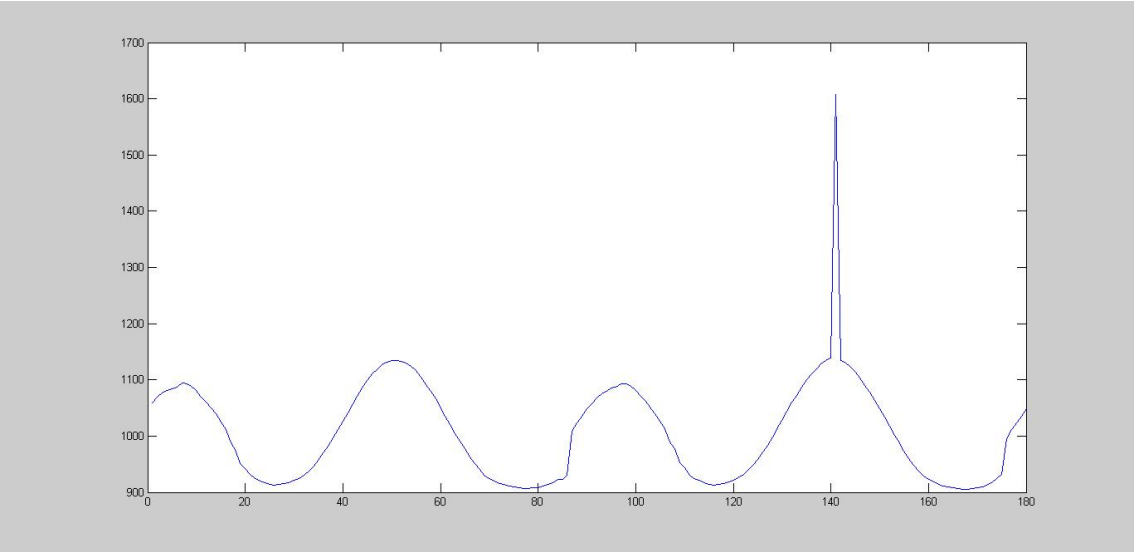

Figure 4.1: Resonance field/Oe against $angle/^o$ of FMR spectrum observed for the 15uc LSMO film at $T = 150K$

The frequency at which resonance occurs in LSMO [90] is expressed as Eq.(2.3.3). Equation

(2.3.3) was derived using the famous Smit and Beljers model. But according to Baselgia et.al (1988) there exists discrepancy in the model which cannot be eliminated and therefore a new model which can eliminate this discrepancy was proposed. The main source of the discrepancy is the origin of the different terms in the free energy, F which is obscured by an angular dependent mixing [57].

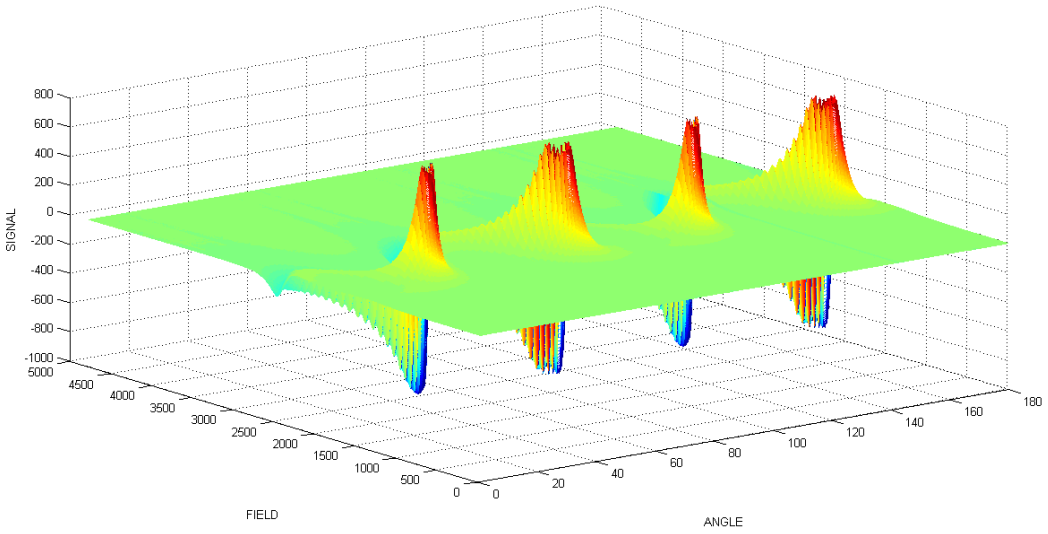

Figure 4.2: Surface plot of 15uc LSMO thin film at $T = 150K$

As can be observed in figure 4.3, there is an increase in the coercive field as the thickness of the three LSMO samples decreases. This is consistent with ref.[150,151]. This increase in the coercive field as the thickness of the LSMO sample decreases is usually towards a thickness which is comparable to the width of the domain wall of LSMO [151]. Also, in figure 4.3, it can be observed that the Curie temperature increases as the thickness of all the three LSMO sample increases. This is in agreement with ref.[99,152]. The increase in Curie temperature as the thickness of the LSMO sample increases is usually towards a thickness which is comparable to the spin-spin correlation length [151].

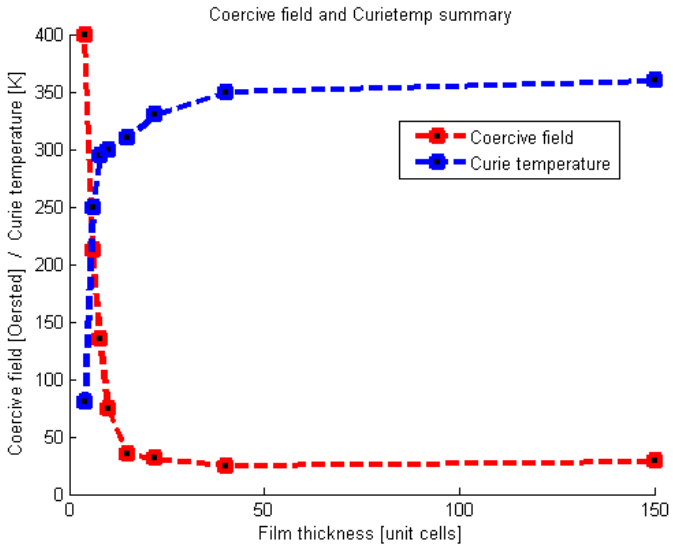

Figure 4.3: Coercive field [Oe]/ Curie temperature[K] vrs film thickness [unit cells] of the LSMO sample at $T = 5K$.

In figure 4.4, it can be observed that as the thickness of the LSMO sample increases, the volume magnetization also increases. This is also consistent with ref.[153,152] in which the magnetization of LSMO thin film which was fabricated on STO substrate at $T = 5K$ was measured.

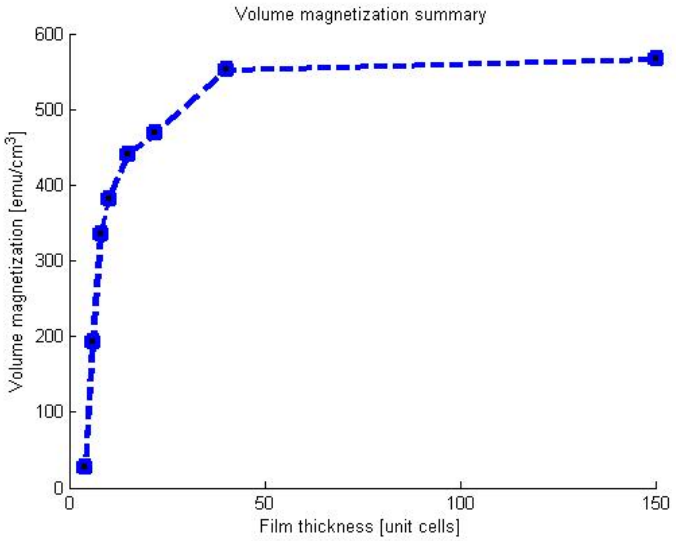

Figure 4.4: Volume magnetization $[emu/cm^3]$ vrs film thickness [unit cells] of LSMO sample at $T = 5K$.

Chapter 5

CONCLUSION AND RECOMMENDATIONS

5.1 CONCLUSION

Ferromagnetic resonance at a temperature, T=150K has been observed in a 15uc thick LSMO thin film. The ferromagnetic resonance spectrum is sinusoidal-like in nature with maximum and minimum curvatures. This maximum and minimum curvatures of the resonance spectrum might be attributed to the singled-value double differentiable function in the resonance equation. The 15uc thick LSMO sample which was deposited on the STO substrate showed unequal resonance field. The center position and the full width half maximum of the 15uc LSMO thin film were 1070.1875 Oe and 159.3125 Oe respectively. The Curie temperature, T_c of the LSMO samples which were measured at temperature, T=5K increases with increasing film thickness whiles the coercive field decreases with increasing film thickness. Also, the volume magnetization of the LSMO samples increases with increasing film thickness.

5.2 RECOMMENDATIONS

Further experiments are required to confirm ferromagnetic resonance in LSMO thin films. This can be achieved when more angular dependence of FMR are carried out on different film

thickness [unit cells] of the LSMO samples. Since ferromagnetic resonance is an experimental technique which can be used in determining the magnetic properties of thin films, magnetic hysteresis measurement can also be performed on the LSMO sample to ascertain its magnetic properties. Further research can also be done on the frequency dependence of the resonance field, H_{res} which determines the gyromagnetic ratio so that the g-factor can also calculated for the LSMO sample. Due to discrepancies between experimental results and theory for the frequency at which resonance occurs using the Smit and Beljers model, the modified model which was proposed by Baselgia et. al (1988), which avoids mixing in the free energy, F which obscures the angular dependent terms can be used instead.

Bibliography

[1] S. Chatterjee, Heisenberg and ferromagnetism (2004), available at http://www.ias.ac.in/resonance/Aug2004/pdf/Aug2004p57-66.pdf

[2] J. Stöhr and H.C. Siegmann. *Magnetism from Fundamental to Nanoscale* . Solid-State Sciences. Springer, 2006

[3] Daniel C. Mattis. *The Theory of Magnetism Made Simple : An introduction to Physical Concepts And To Some Useful Mathematical Methods*. World Scientific Publishing Co. Pte. Ltd, 2006

[4] Edward Nevile Da Costa Andrade. The Early History of the Permanent Magnet. 17(65): 1-9, January, 1958

[5] Oleksandz Mosendz. Dynamics in Ultrathin Magnetic Fields. PhD Thesis, 2002

[6] Mathias Getzlaff. *Fundamentals of Magnetism*. Springer, 2008.

[7] Gregory A. Landrum and Richard Dronskowsi. Ferromagnetism in Transition Metals : A Chemical Bonding Approach. *Angew. Chem. Int. Eds*, 38(10) : 1389-1393, 1999

[8] R.O. Zaitsev. Theory of Ferromagnetism for Metals of Cubic Symmetry. *JETP Letters*, 72(2): 109-114, 2000

[9] Lecture notes on Itenerant Ferromagnetism. Retrieved on 4/01/2011 at

[10] B. Chatterjee. Oxidation of Iron, Cobalt and Nickel at Curie temperature. *Solid State Communication*, 27: 1455-1458, 1978

[11] J.M.D. Coey. *Magnetism and Magnetic Materials*. Cambridge University Press, 2010

[12] The discovery of Giant Magnetoresistance. Compiled by the Class for Physics of the Royal Swedish Academy of Sciences, 17(6), 2007

[13] C. Chappert, D. Renard, P. Beauvillain, J.P. Renard and J. Seiden. Ferromagnetism of very thin films of nickel and cobalt. *Journal of Magnetism and Magnetic Materials*: 54-57, 1986

[14] J.C. Sankey, P.M. Braganca, A.G.F. Garcia, I.N. Krivorotov, R.A. Buhrman and D.C. Ralph. Spin-Transfer-Driven Ferromagnetic Resonance of Individual Nanomagnets. *Physical Review Letters*, PRL 96: 227601, 9 June, 2006

[15] Charles Kittel. On the Theory of Ferromagnetic Resonance Absorption. *Physical Review*, 73(2): 155-161, 15 January, 1948

[16] Mikihiko Oogane, Takeshi Wakitani, Satoshi Yakata, Resul Yilgin, Yasuo Ando, Akimasa Sakuma and Terunobu Miyazaki. Magnetic Damping in Ferromagnetic Thin Films. *Japanese Journal of Applied Physics*, 45(5A): 3889-3891, 2006

[17] Michael Farle. Ferromagnetic resonance of ultrathin metallic layers. *Rep. Prog. Phy.*, 61: 755-826, 1998

[18] J.M. Beaujour, D. Ravelosona, I. Tudosa, E.E. Fullerton and A.D. Kent. Ferromagnetic resonance linewidth in ultrathin films with perpendicular magnetic anisotropy. *Physical Review B*, 80: 180415(R), 2009

[19] P. Poulopoulos and K. Baberschke. Magnetism in thin films. *J. Phys: Condens. Matter*, 11, 1999

[20] M.T. Johnson, P.J.H. Bloemen, F.J. de Broeder and J.J. de Varies. Magnetic anisotropy in metallic multilayers. *Rep. Prog. Phys.*, 59: 1409-1458, 1996

[21] Chun-Gang Duan, Julian P. Velev, R.F. Sabirianov, W.N. Mei, Sitaram Jaswal and Evgeny Y. Tsymbal. Tailoring Magnetic Anisotropy at the Ferromagnetic / Ferroelectric Multilayers. *Applied Physics Letters*, 92: 122905, 2008

[22] Mattieu Jamet, Wolfgang Wernsdorfer, Christopher Thirion, V'eronique Dupuis, Patrice M'elinon, Alain Pe'rez and Dominique Mailly. Magnetic Anisotropy of Magnetic in Single Clusters. *Physical Review B*, 69, 2004

[23] A.A. Kusov, S.S. Jaswal and Z.S. Shan. Shape Anisotropy of Magnetic Multilayers. *Physical Review B*, 46(5): 3123-3124, 1 August, 1992

[24] Ding-sheng Wang, Ruquian Wu, A.J. Freeman. First-Principle Theory of Surface Magnetocrystalline Anisotropy and Diatomic-pair Model. *Physical Review B*, 47(22): 14932-14947, 1 May, 1993

[25] O. Eriksson and J. Wills. First Principle Theory of Magnetocrystalline Anisotropy. Springer, 1999

[26] A.S. Kamzin, V.L. Rozenbaum and L.P. Ol'khovik. Investigation of magnetic structure and volume of aluminium -substituted Sr-M type hexaferrites. *JETP LETTERS*, 67 (10): 843-847, 25 May, 1998

[27] M. Rickart, T. Mewes, S.O. Demokritov, B. Hillerbrands and M. Scheib. Correlation between topography and magnetic surface anisotropy in epitaxial Fe films on vicinal-to-(001) Au surfaces with different step orientation. *Physical Review B*, 70: 060408(R), 2004

[28] Ulrich Gradmann. Magnetic Surface Anisotropies. *Journal of Magnetism and Magnetic Materials*: 54-57, 1986

[29] M.A.M. Gijs and F. Petroff. Magnetic Ultra Thin Film, Multilayers and Surface. Elsevier Science BV, 1997

[30] H.J. Elmers amd U. Gradmann. Dependence of magnetic surface anisotropies on symmetries of a nonmagnetic overlayer. *Surface Science*, 304: 201-207, 1994

[31] U. Gradmann and H.J. Elmers. Magnetic surface anisotropies in NiFe-alloy films : Separation of intrinsic Néel type from strain relaxation contributions. *Journal of Magnetism and Magnetic Materials*, 206 : L107-L112, 1999

[32] G. Bayreuther. Magnetic Surfaces. *Hyperfine Interaction*, 47: 237-249, 1989

[33] P. Bruno and J. Seiden. Theoretical Investigation on Magnetic Surface Anisotropy. *Journal of Physics*, 49(12): C81645-C81646, 1988

[34] P. Bruno and J.P. Renard. Magnetic surface anisotropy of transition metal ultrathin films. *Appl. Phys. A*, 49: 499-506, 1989

[35] Hari Singh Nalwa. *Handbook of Thin Film Materials*. Academic Press, 2002

[36] Klaus Baberschke. Novel Techniques for Characterization and Preparing Samples. *John Wiley and Sons, Ltd*, 2007

[37] Yaroslav Tserkovnyak, Arne Brataas, Gerrit E.W. Bauer and Bertrand I. Halperin. Nonlocal Magnetization Dynamics in Ferromagnetic Heterostructures. *Reviews of Modern Physics*, 77: 1375-1418, October, 2005

[38] R. Urban, G. Woltersdorf and B. Heinrich. Gilbert Damping in Single and Multilayer Ultrathin Films : Role of Interfaces in Nonlocal Spin Dynamics. *Physical Review*, 87 (21): 217204, 19 November, 2001

[39] Douglas L. Mills and Sergio M. Rezende. Spin Damping in Ultrathin Magnetic Films. *Appl Phys.*, 87(59): 27-58, 2003

[40] Robert D. McMichael and Pavol Krivosik. Classical Model of Extrinsic Ferromagnetic Resonance Linewidth in Ultrathin Films. *Classical Transactions on Magnetics*, 40(1), 1 January 2004

[41] M. Lakshmanan. The Fascinating World of Landau-Lifshitz-Gilbert Equation. *An Article Submitted to the Royal Society*: 1-21, 2011

[42] Dana Elena Sorea Stanescu. Magnetization Dynamics in Magnetic Nanostuctures. *PhD thesis submitted to the Department of Physics.* Joseph Fourier University, 2004

[43] M. Lakshmanan and K. Nakamura. Landau-Lifshitz- Equation of Ferromagnetism : Exact Treatment of the Gilbert Damping. *Physical Review Letters*, 53 (26): 2497-2499, 24 December, 1984

[44] Thomas Bose and Steffen Trimper. Correlation Effects in the Stochastic Landau-Lifshitz-Gilbert Equation. *Physical Review B*, 81: 104413, 2010

[45] K. Lenz, K. Wende, W. Kuch, K. Baberschke, K. Nagy and A. Jánossy. Two -Magnon Scattering and Viscous Gilbert Damping in Ultrathin Ferromagnets. *Physical Review B*, 73: 144424, 2006

[46] Chunsheng Liu, Claudia K.A. Mewes, Mairbek Chshiev, Tim Mewes and William H. Butler. Origin of Low Damping in Half Metals. *Applied Physics*, 95: 022509, 2009

[47] M.C. Hickey and J.S. Moodera. Origin in Intrinsic Gilbert Damping. *Physical Review Letters*, PRL 102: 1-5, 2009

[48] Chein-Shan Liu. Lie symmetry of the Landau-Lifshitz-Gilbert equation and exact linearization in the Minkowski space. *Z. angew. Math. Phys.*, 55: 606-625, 2004

[49] Shufeng Zhang and Steven S.L. Zhang. Generalization of the Landau-Lifshitz- Gilbert Equation for Conducting Ferromagnets. *Physical Review Letters*, PRL 102: 086601, 27 February, 2009

[50] Nobuyuki Umetsu, Daisuke Miura and Akimasa Sakuma. Microscopic theory on the Gilbert damping due to spin pumping effects in the magnetic multi-layer system. *Journal of Physics : Conference Series 266*: 012084, 2011

[51] N. Vukadinovic, M. Labrune, J. Ben Youssif, A. Martey, J.C. Toussaint and H.Le Gell. Ferromagnetic resonance spectra in a weak stripe domain structure. *Physical Review B*, 65: 054403, 2001

[52] D. Polder. On the Quantum Theory of Ferromagnetic Resonance. *Letters to the Editor*, 2 March, 1948

[53] Jeffery MacLeod Rudd. Ferromagnetic Resonance in Nickel at Low Temperatures. *MSc. Thesis submitted to the Department of Physics*, Simon Fraser University, 1981

[54] J. Lindner and Baberschke. Ferromagnetic resonance in coupled ultrathin films. *J. Phys.: Condens. Matter*: 15: S465-S478, 2003

[55] B. Heinrich and J.A.C Bland. Ultrathin Magnetic Structures ii. *Springer*, 1994

[56] Z. Celinski, K.B. Urquarant and B. Heinrich. Using ferromagnetic resonance to measure the magnetic moments of ultrathin films. *Journal of Magnetism and Magnetic Materials*, 166: 6-26, 1997

[57] L. Baselgia, M. Warden, F. Walder, Stuart L. Hutton, John E. Drumheller, Y. Q. He and P.E. Wigen. Derivation of the resonance frequency from the free energy of ferromagnets. *Physical Review B*, 38(4): 2237-2242, 1 August, 1988

[58] R.F. Sekerka. Ferromagnetic resonance frequency in anisotropic crystals for arbitrarily field. *Physics Letters*, 29A(9): 560-561, 30 May, 1969

[59] S.E. Bushnell, W.B. Nowak, S.A. Oliver and C. Vittoria. The measurement of magnetostriction constants of thin films using microwave devices and ferromagnetic resonance. *Rev. Sci. Instum*, 63(3): 2021-2025, 01 March, 1992

[60] A. Layadi. Ferromagnetic resonance modes in single and coulped layers with oblique anisotropy axis. *Physical Review B*, 63: 174410, 2001

[61] Dinsh Martien. Introduction to: AC Susceptibility. *Quantum Design*, 2006

[62] Sangita S. Kalarickal, Pavol Krivosik, Mingzzhong Wu, Car E. Patton, Pavel Kabos and T.J. Silva. Ferromagnetic resonance linewidth in metallic thin films: Comparison of measurement methods. *Journal of Applied Physics*, 99 : 093909, 2006

[63] J. Tudor Davies. Effect of Nonuniform Magnetization of the Spin-Wave Spectrum in Thin Films Ferromagnetic Films. *Journal of Applied Physics*, 35(3): 804-805, March, 1964

[64] P.C. Fannin, I. Malaescu and C.N. Marin. Determination of the Landau-Lifshitz damping parameters of composite magnetic fluids. *Physica B*, 388: 93-98, 2007

[65] S.E. Harrison, H.S. Belson and C.J. Kriessman. Origin of ferromagnetic resonance line in manganese-rich manganese ferrites. *Journal of Applied Physics*, 29(3): 337-338, March, 1958

[66] J. Lindner, I. Barsukov, C. Raeder, C. Hassel, O. Posth, R. Meckenstock, P. Landerous and D.L. Mills. Two-magnon damping in thin films in case of canted magnetization : Theory and Experiment. *Physical Review B*, 80: 224421, 2009

[67] D.L. Mills and Rodrigo Arias. The damping of spin motions in ultrathin films : Is the Landau-Lifshitz-Gilbert phenomenology applicable? *J. Appl. Phys.*, 87, 2005

[68] Jamal Ben Youssef and Christian Brosseau. Magnetization damping in two component metal oxide micropowder and nanopowder compacts by broadband ferromagnetic resonance measurements. *Physical Review B*, 74: 214413, 2006

[69] R. Meckenstock, D. Spoddig, Z. Frait, V. Kambersky and J. Pelzl. Anisotropic Gilbert damping in epitaxial Fe films on InAs(001). *Journal of Magnetism and Magnetic Materials*: 272-276, 2004

[70] A.P. Ramirez. Colossal Magnetoresistance. *J. Phys.: Condens. Matter*, 9: 8171-8199, 1997

[71] J.M.D. Coey, M. Viret and S. Von Molnar. Mixed -Valence Manganites. *Advances in Physics*, 48(2): 167-293, 1999

[72] A.M. Haghiri and J.P. Renard. CMR Manganites : physics, thin films and devices. *J. Phys. D. : Appl. Phys.*, 36: R127-R150, 2003

[73] C.S. Nelson, V. Kiryukhin, J.P. Hill and Doon Gibbs. Structural Correlation and Colossal Magnetoresistance Effect. *NSLS Activity Report*, 2001

[74] Y. Chen, B.G. Ueland, J.W. Lynn, G.L. Bychkov, S.N. Barilo, Y.M. Mukovskii. Polaron formation in the optimally doped ferromagnetic manganites $La_{0.7}Sr_{0.3}MnO_3$, and $La_{0.7}Ba_{0.3}MnO_3$. *Physical Review B*, 78 : 212301, 2008

[75] R.V. Demin, L.I. Koroleva and Ya M. Mukovskii. Giant Volume Magnetostriction and Colossal Magnetoresistance at room temperature in $La_{0.7}Ba_{0.3}MnO_3$. *J. Phys.: Condens. Matter*, 17:221-226, 2005

[76] Dmitry Ruzmetov, Yongho Seo, Land J. Belenky, D.M. Kim, Xianglin Ke, Haiping Sun, Venkat Chandransekhar, Chang-Beom Eom, Mark S. Rzcowski and Xiaqimg Pan. Epitaxial magnetic perovskite nanostructures. *Advanced Materials* : 1-15, 2005

[77] T. Manabe, T. Fujimoto, I. Yamaguchi, W. Kondo, I. Kojima, S. Mizuta and T. Kumagai. Effects of substrate materials and annealing temperature on crystal structure and epitaxy of $La_{0.7}Sr_{0.3}MnO_3$ films via dipping-pyrolysis process. *Thin Solid Films*, 323: 99-104, 1998

[78] S. Brivio, M. Cantoni, D. Petti, A. Cattoni, R. Bertacco, M. Finazzi, F. Ciccacci, A. Sidorenko, G. Allodi, M. Ghidini and R. de Renzi. Decrease of the Curie temperature in $La_{0.7}Sr_{0.3}MnO_3$ thin films induced by Au capping. *Materials Science and Engineering B*, 144: 93-96, 2007

[79] N. Farag, M. Bobeth, W. Pompe, A.E. Romanov and J.S. Speck. Rhombohedral LSMO films- a unique case of ferroelectricity domain formation. *Phys. Stat. Sol.* (a)202 (4): R44-R46, 2005

[80] G. Banach and W.M. Temmerman. Delocalization and charge disproportionation in $La_{1-x}Sr_xMnO_3$. *Physical Review B*, 69: 054427, 2004

[81] Ayan Ray, Debashis Panda, Tamita Rakshit, Sanjay K. Mandal, Indranil Manna and Samit K. Ray. Growth and Optical Properties of $La_{0.7}Sr_{0.3}MnO_3/ZnO$ Heterojunction. *2nd International Workshop on Electron Devices and Semiconductor Technology*: 1-4, 2009

[82] San Ping Jiang. Development of lanthanum strontium perovskite cathode materials of solid oxide fuel cells: a review *J. Mater Sci.*, 43: 6799-6833, 2008

[83] L. Martín- Carrón, A. de Andrés, Martínez, M.T. Casais and J.A. Alonso. Raman phonons as a probe of disorder, fluctuations and local structure in doped and undoped orthorhombic and rhombohedral manganites. *Physical Review B*, 66: 174303, 2002

[84] K. Horiba, A. Chikamatsu, H. Kumigashira, M. Oshima, H. Wadati, M. Lippmaa, M. Kawasaki and H. Koinuma. Temperature-dependence of electronic structure $La_{1-x}Sr_xMnO_3$ thin films studied by in-situ photoemission spectroscopy. *Journal of Electron Spectroscopy and Related Phenomena*: 156-158, 2007

[85] A.K. Pradhan, J.B. Dadson, D. Hunter, Z. Zhang, S. Mohanty, E.M. Jackson, B. Lasley-Hunter, K. Lord, T.M. Williams, R.R. Rakhimov, J. Zhang, D.J. Sellmyer, K. Inaba, T. Hasegawa, S. Mattews, B. Joseph, B.R. Sekhar, U.H. Roy, Y. Cui and A. Burger. Ferromagnetic properties of epitaxial manganite films on $SrTiO_3/Si$ heterostrutures. *Journal of Applied Physics*, 100: 033903, 2006

[86] Carlos Martínez-Boubeta, Zorica Konstantinoviç, LIuis Balcells, Sonia Estradé, Jordi Arbiol, Alfonso Cebollada and Benjiman Martínez. Epitaxial Integration of $La_{\frac{2}{3}}Sr_{\frac{1}{3}}MnO_3$ and Fe films by the use of a MgO spacer. *Crystal Growth and Design*, 10(3): 1017-1020, 2010

[87] Tetsu Uemura, Kenji Sekine, Ken-ichi Matsuba and Masafumi Yamamoto. Magnetic and Electrical Properties of $(La, Sr)MnO_3$ sputtered on $SrTiO_3$-Buffered Si Substrate. *Japanese Journal of Applied Physics*, 44(4B): pp 2604-2607, 2005

[88] H.L. Liu, M.X. Kuo, J.L. Her, K.S. Weng, L.M. Wang, S.L. Cheng and J.G. Lin. Thickness-dependent optical properties of $La_{0.7}Sr_{0.3}MnO_3$ thin films. *Journal of Applied Physics*, 97: 113528, 2005

[89] A.K. Pradhan, D. Hunter, T. Williams, B. Lasley-Hunter, R. Bah, H. Mustafa, R. Rakhimov, J. Zhang, D.J. Sellmyer, E.E. Carpenter, D.R. Sahu and J.L. Huang. Magnetic properties of $La_{0.6}Sr_{0.4}MnO_3$ thin films on $SrTiO_3$ and buffered Si substrates with varying thickness. *Journal of Applied Physics*, 103: 023914, 2008

[90] R. Bah, D. Bitok, R.R. Rakhimov, M.M. Noginov, A.K. Pradhan and N. Noginova. Ferromagnetic resonance studies on colossal magnetoresistance films : Effects of homogeneity and light illumination. *Journal of Applied Physics*, 99: 08Q312, 2 November, 2006

[91] Joo-Hyung Kim, Alexander M. Grishin, Herry H. Radamson. Properties of $La_{0.75}Sr_{0.25}MnO_3$ films grown on Si substrate with $Si_{1-x}Ge_x$ and $Si_{1-y}C_y$ buffer layers. *Thin Solid Films*, 515: 411-415, 2006

[92] D.W. Kim, T.W. Noh, H. Tanaka and T. Kawai. Influence of microstuctures of exchange bias behaviors of $La_{0.7}Sr_{0.3}MnO_3$ / $La_{0.33}Ca_{0.67}MnO_3$ bilayers. *Solid State Communication*, 125: 305-309, 2003

[93] S. Iwasaki, M. Tada, J. Yamada, Y. Inamori, J. Nogués and T. Endo. Temperature dependence of FMR of La-Ba-Mn-O thin films. *Physica B*: 329-333, 2003

[94] Mahmoud Al Ahmad, Eiu-Jung Yun, Char II Cheon and Robort Plana. Tunability of Ferromagnetic $(La, Sr)MnO_3$ (LSMO) Thin Films for Microvave Applications. *Proceedings of the 38th European Microwave Conference*: 1296-1299, October, 2008

[95] Y.P. Liu, Y.S. Du, M. Zhang, H. Yan and Y.Y. Wang. Effect of internal strain on magnetic properties of $La_{0.7}Sr_{0.3}MnO_3$ films. *Vacuum*, 81: 826-829, 2007

[96] I. Bergenti, V. Dediu, M. Cavallini, E. Arisi, A. Riminucci and Taliani. Properties of thin films grown on semiconducting substrates for spintronic applications. *Current Applied Physics*, 7: 47-50, 2007.

[97] M. Bibes, K. Bouzehouane, A. Barthélémey, M. Besse, S. Fusil, M. Bowen, P. Seneor, J. Carry, V. Cros, A. Vaurés, J.P. Contour and A. Fert. Tunnel Magnetoresistance and Nanojunctions based on Sr_2FeMoO_6. *Applied Physics Letters*, 83(13): 2629-2631, 29 September, 2003

[98] J.C. Jiang, E. I.Meletis, and K.I. Gnanasekar. Self-organized, ordered array of coherent orthogonal column nanostructures in epitaxial $La_{0.8}Sr_{0.2}MnO_3$ thin films. *Applied Physics Letters*, 80(25): 4831-4833, 24 June, 2002

[99] Bongju Kim, Daeyoung Kwon, Jong Hyun Song, Yasuyuki Hikita, Bog G. Kim and Harold Y. Hwang. Finite size effect and phase diagram of ultrathin $La_{0.7}Sr_{0.3}MnO_3$ thin films. *Solid State Communications*, 150: 598-601, 2010

[100] S. Brivio, C. Magen, A.A. Sidorenko, D. Petti, M. Cantoni, M. Ciccacci, R. De Renzi, M. Varela, S. Picozzi and R. Bertacco. Effects of Au nanoparticles on the magnetic and transport properties of $La_{0.67}Sr_{0.33}MnO_3$ ultrathin layers. *Physical Review B*, 81: 094410, 2010

[101] S.H. Seo, H.C. Jang and D.Y. Noh. Effects of oxygen incorporation in tensile $La_{0.84}Sr_{0.16}MnO_{3-\delta}$. *Physical Review B*, 71: 012412, 2005

[102] O.I. Lebedev, G. Van Tendeloo and S. Amlincky. Misfit accomodation of epitaxial $La_{1-x}A_xMnO_3(A = Ca, Sr)$ thin films. *International Journal of Inorganic Materials*, 3: 1331-1337, 2001

[103] Chunlan Ma, Zhongqin Yang and Silvia Picozzi. Ab initio electronic and magnetic structure in $La_{0.66}Sr_{0.33}MnO_{3-\delta}$: strain and correlation effects. *J. Phys. : Condens. Matter*, 18: 7717-7728, 2006

[104] D.R. Sahu, D.K. Mishra, Jow-Lay Huang, B.K. Roul. Annealing effect on properties of $La_{0.7}Sr_{0.3}MnO_3$ thin film grown on Si substrate by DC sputtering. *Physical B*, 396: 75-80, 2007

[105] M. Okaji. Absolute Thermal Expansion Measurement of Single-Crystal Silicon in the range 130-1300 K with an Interferometric Dilatometer. *International Journal of Thermophysics*, 9(6): 1101-1109, 1988

[106] Manh-Huong Phan, Seong-Cho Yu, A.N. Ulyanov and H.K. Lachowich. Large magnetocaloric effect in perovskite manganites : changes of the magnetic entropy above 300K. *Material Science*, 21(1): 133-139, 2003

[107] Soma Das and T.K. Dey. Magnetic effect in potassium doped lanthanum manganite perovskites prepared by a pyrophoric method. *J. Phys.: Condens. Matter*, 18: 7629-7641, 2006

[108] Hideaki Sakai, Yaujiro Taguchi and Yoshinori Tokura. Impact of Bicritical Fluctuation of Magnetocaloric Phenomena in Perovskite Manganites. *Journal of the Physical Society of Japan*, 78(11): 113708, November, 2009

[109] M. El-Hagary, Y.A. Shoker, M. Emam-Ismail, A.M. Moustafa, A. Abd El-Aal, A.A. Ramadam. Magnetocaloric effect in manganite perovskites $La_{0.77}Sr_{0.3}Mn_{1-x}Cu_xO_3$ ($0.1 \leqslant x \leqslant 0.3$). *Solid State Communications*, 149: 184-187, 2009

[110] M. Izuma, Y. Ogimoto, Y. Konishi, T. Manako, K. Kawasaki and Y. Tokura. Perovskite superlattices as tailored materials of correlated electrons. *Material Science and Engineering B*, 84: 53-57, 2001

[111] G. Van Tendeloo, O.I. Lebedev and S. Amelinckyx. Atomic and microstruture of CMR materials. *Journal of Magnetism and Magnetic Materials*, 211: 73-83, 2000

[112] R. Govindaraj and C.S. Sundar. Implications of Mn site hyperfine fields on CMR properties of manganites as studied by perturbed angular correlation spectroscopy. *Phys. Scr.*, 74: 247-250, 2006

[113] Yen-Hua Chen, Shu-Te and Tai-Bor Wu. Conductive AFM of Percolative Metal-Insulator Transition in Polycrystalline $La_{0.91}Sr_{0.09}MnO_3$ Thin Films Deposited on Si Substrate. *Electrochemical and Solid-State Letters*, 9(7): J27-J30, 2006

[114] T. Kageyama, T. Hasegawa, T. Koida, M. Ohtani, T. Fukumura, M. Kasawaki and H. Koinuma. Local magnetic measurements of composition-spread manganese oxide thin films with a scanning SQUID microscope. *Appl. Phys.A*, 72 [Suppl]: S273-S276, 2001

[115] Zhong Fang and Kiyoyuki Terakura. Surface Magnetic Phase Diagram of Tetrahedral Manganites. *Journal of the Physical Society of Japan*, 70(11) : pp 3356-3361, November, 2001

[116] Osamu Kohmoto. Ferromagnetic resonance of amorphous Fe wire. *Material Science and Engineering A* : 449-451, 2007

[117] Yolanda Y. Villanueva, Da-Ren Liu and Pei Tzu Cheng. Pulsed Laser Deposition of Zinc Oxide. *Thin Solid Films*, 501: 366-369, 2006

[118] http://tauvex.iiap.res.in/tauwiki/index.php/Image:SphericalCoordinates.gif

[119] A. Tebano, C. Aruta, P.G. Medaglia, F. Tozzi, G. Balestrino, A.A. Sidorenko, G. Allodi, R.De Renzi, G. Ghiringhelli, C. Dallera, L. Braicovich and N.B. Brookes. Strain -induced separation in $La_{0.7}Sr_{0.3}MnO_3$ thin films.*Physical Review B*, 74: 245116, 2006

[120] Zhi-Hong Wang, H. Kronmüller, O.I. Lebedev, G.M. Gross, H.U. Habermeier and B.G. Shen. Phase transition and magnetic anisotropy of $(La, Sr)MnO_3$. *Physical Review B*, 65 : 054411, 2002

[121] M. Huijben, L.W. Martin, Y.H. Chu, M.B. Holcomb, P.Yu, G. Rijnders, D.H.A. and R. Ramesh. Critical thickness and orbital ordering in ultrathin $La_{0.7}Sr_{0.3}MnO_3$ films. *Physical Review B*, 78: 094413, 2008

[122] G. Alejandro, L.B. Steren, H. Pastoriza, D. Vega, M. Granada, J.C. Rojas Sanchez, M. Sirena and B. Alascio. Magnetoresistance effect in $(La, Sr)MnO_3$ bicrystalline films. *J. Phys.: Condens. Matter*, 22 : 346007(10pp), 2010

[123] C. Kwon, S.E. Lofland, S.M. Bhagat, M. Rajeswari, T. Venkatsan, R. Ramesh, A.R. Kratz and R.D. Gomez. Stress-Induced Surface Magnetization of $La_{0.7}Sr_{0.3}MnO_3$ Thin Films. *IEEE Transactions on Magnetics*, 33(5): 3964-3966, September, 1997

[124] J.M.L Beaujour, W. Chen, A.D. Kent and J.Z. Sun. Ferromagnetic resonance study of polycrystalline cobalt ultrathin films. *Physical Review B*, 21(5): 1-3, 2008

[125] A.N. Pogorily, A.I.T. Tovstolytkin, I.V. Lenhnenko, A.I. Motvienko and D.I. Pod'yalovsky. Peculiar magnetic and magnetoresistive properties of $La_{0.7}Sr_{0.3}MnO_{3-\delta}$ polycrystalline thin films. *Functional Materials*, 10(1): 30-33, 2003

[126] Maksym Sladkov. Electronic detection study of magnetization dynamics in ferromagnetic/nonmagnetic systems. Master Thesis, 2006

[127] Y. Suzuki, H.Y. Hwang, S.W. Cheong and R.B. van Dover. The role of strain in magnetic anisotropy of manganite thin films. *App. Phys. Lett.*, 71(1): 140-142, 7 July, 1997

[128] P. Landerous, Rodrigo E. Arias and D.L. Mills. Two magnon scattering in ferromagnets : The case where the magnetization is out of the plane. *Physical Review*, B 77, 214405, 2008

[129] M.T. Causa, M. Tovar, A. Caneiro, F. Prado, G. Ibane, C.A. Ramos, A. Butera, B. Alascio, X. Obradors, S. Pinol, F. Rivadulla, C. Vázquez-Vázquez, M.A. López-Quintela, J. Rivas, Y. Tokura and S.B. Oseroff. High-temperature spin dynamics in CMR manganites : ESP and magnetization. *Physical Review B*, 58(6): 3233-3239, 1 August,1998

[130] R.D. McMichael, M.D. Stiles, P.J. Chen and W.F. Egelhoff, Jr. Ferromagnetic resonance studies of NiO-coupled thin films of $Ni_{80}Fe_{20}$. *Physical Review B*, 58(13): 8605-8612, 1 October,1998

[131] Resul Yilgin, Mikihiko Oogane, Stoshi Yakata, Yasuo Ando and Terunobu Miyazaki. Gilbert Damping constant in Co_2MnAl Heusler Alloy Films. *IEEE TRANSACTIONS OF MAGNETICS*, 41(10): 2799-2801, October, 2005

[132] Z. Celinski and B. Heinrich. Ferromagnetic resonance linewidth of Fe ultrathin films grown on a bcc Cu substrate. *J. Appl. Phys.*, 70(10): 5935-5937, 1991

[133] V.A. Atsarkin, V.V. Demidov and A.M. Balbashov. Anomalous Slowing Down of the Longitudnal Spin Relaxation near the Antiferromagnetic Phase Transition in $LaMnO_3$ Manganite. *JETP Letters*, 80(9): 593-596, 2004

[134] Yi Li, M. Farle and K. Baberschke. Critical spin fluctuations and Curie temperature of ultrathin film Ni(111)/W(110): A magnetic -resonance study in ultrathin vacuum. *Rapid Communications Physical Review B*,41(13): 9596-9599, 1 May, 1990

[135] C. Rettori, D. Rao, J. Singley, D. Kidwell, S.B. Oseroff, M.T. Causa, J.J. Neumeier, K.J. McClellan, S.W. Cheong and S. Schultz. Temperature dependence of the ESR linewidth in the paramagnetic phase ($T > T_c$) of $R_{1-x}B_xMnO_{3+\delta}(R = La, Pr; B = Ca, Sr)$. *Physical Review B*, 55(5): 3083-3086, 1 Feb,1997

[136] Battogtokh Jugdersuren, Sungmu Kang, Robert S. DiPietro, Don Heiman, David McKeown, Lan. L. Pegg and John Philip. Large low field magnetoresistance in $La_{0.67}Sr_{0.33}MnO_3$ nanowire devices. *Journal of Applied Physics*, 109 : 016109, 2011

[137] N.M. Salansky, B.P. Khrustalev, A.S. Melnik, L.A. Salanskaya and Z.I. Sinegubova. Ferromagnetic resonance linewidth in thin magnetic films. *Thin Solid Films*, 4 : 105-133, 1969

[138] J. Jiménez-Jarquin, E. Haro-Poniatowski, M. Fernandez-Guasti and J.L. Hernandez-Pozos. Laser induced microstructuring of silicon under different atmosphere. *Radiation Effects and Defects in Solids*, 164(7-8): 443-451, July-August 2009.

[139] L.E. Gontchar and A.A. Mozhegorov. Magnetic structure and antiferromagnetic resonance spectrum in manganites : The effect of orbital structure. *Physical Review*, 47(8): 1455-1458, 2005

[140] J.H. Westbrook and R.L. Fleischer. *Intermetallic Compounds-Principles and Practice: Progress*. John Wiley and Sons Ltd, volume 3 : 167-177, 2002

[141] G. Alejandro, M.C.G. Passeggi, D. Vega, C.A. Ramos, M.T. Causa, M. Tovar and R. Senis. Temperature evolution of crystal field interactions across the Jahn-Teller transition in a $La_{\frac{7}{8}}Sr_{\frac{1}{8}}MnO_3$ single crystal. *Physical Review B*, 68: 214429, 2003

[142] G. Counil, Joo-Von Kim, C. Chappert, K. Shigeto and Y. Otani. Spin wave contributions to the high-frequency magnetic response of thin films obtained with inductive methods. *Journal of Applied Physics*, 95(10), 15th May 2004

[143] X. Liu, Y.Y. Zhou and J.K. Furdyna. Angular dependence of spin wave resonances and surface spin pinning in ferromagnetic (Ga,Mn) As films. *Physical Review B*, 75: 195220, 2007

[144] M. Mizuguchi and K. Takanashi. Ferromagnetic resonance of Fe nanodots grown on MgO measured using coplanar waveguides. *J. Phys. D: Appl. Phys.*, 44: 064007, 2011.

[145] Mikhail Kostylev, Rhet Magaraggia, Feodor Y. Orgin, Evgeny Sirotkin, Vladimir F. Mescheryakov, Nils Ross and Robert L. Stamps. Ferromagnetic resonance investigation of microscopic arrays of magnetic nanoelements fabricated using polysterene nanosphere lithographic mask technique. *IEEE TRANSACTION ON MAGNETICS*, 44(11), Nov. 2008

[146] Anul K. Srivastava, Michael J. Hurben, Michael A. Wittenauer, Pavel Kabos, C. E. Patton, R. Ramesh, Paul C. Dorsy and Douglas B. Chrisey. Angle dependence of the ferromagnetic resonance linewidth and two magnon loses in pulsed laser deposited films of yttrium iron garnet, MnZn ferrite and NiZn ferrite. *Journal of Applied Physics*, 85(11), 1 June 1999.

[147] T. Moriyama, X. Fan, Y. Q. Wen, H.W. Zhang and John Q. Xiao. Ferromagnetic resonance spectroscopy with very larger precession cone angle in magnetic tunnel junctions. *IEEE TRANSACTION ON MAGNETICS*, 44(5), 5 May 2009.

[148] JinJie Jiang and Ralph T. Weber(2001). *Elexsys E 500 User's Manuel: Basic Operations*. Manuel Version 2.0, Software Version 2.1, Bruker Instruments, Inc

[149] M. Belmeguenai, S. Mercone, C. Adamo, T. Chauveau, L. Méchin, P. Monod, P. Moch and D.G. Schlom. $La_{0.7}Sr_{0.3}MnO_3$ thin films on $SrTiO_3$ and $CaTiO_3$ buffered Si substrate : structural, static, and dynamic magnetic properties. *J Nanopart Res*: DOI 10.1004, 18 March 2011

[150] L.B. Steren, M. Sirene and J. Guimpel. Substrate effect on the magnetic behavior of manganite films. *Journal of Applied Physics*, 87(9): 6755-6757, 1 May 2000

[151] R.K. Das, R. Misra, S. Tongay, R. Rairigh and A.F. Hebard. Finite size effects with variable range exchange coupling in thin film $Pd/Fe/Pd$ trilayers. *Journal of Magnetism and Magnetic Materials*, 322: 2618-2621, 2010

[152] C.C. Abilio, M. Rosena, C. Dubourdieu, F. Weiss, K. Fröhlich and M. Godinho. Effect of magnetic field orientation of magnetization of $(La_{0.7}Sr_{0.3}MnO_3/SrTiO_3)_{15}$ superlattices. *Journal of Magnetism and Magnetic Materials* : 272-276, 2004

[153] M. Sirena, L. Steren and J. Grimpel. Thickness dependence of the properties of $La_{0.6}Sr_{0.4}MnO_3$ thin films. *Superficies y Vacío*, 9: 188-192, December 1999.

[154] Hans Boschker, Jaap Kautz, Evert P. Houwman, Gertjan Koster, Dave H.A. Blank and Guus Rijnders. Magnetic anisotropy and magnetization reversal of $La_{0.67}Sr_{0.33}MnO_3$ thin films on $SrTiO_3$ (110). *Journal of Aplied Physics*, 108: 103906, 2010

List of Abbreviations and Constants

C- speed of light

μ_o - permeability of free space

ε_o - permittivity of free space

F_L - Lorentz force

E - electric field

H - magnetic field

FMR - ferromagnetic resonance

γ - gyromagnetic ratio

LL - Landau-Lifshitz

LLG - Landau-Lifshitz - Gilbert

MAE - magnetic anisotropy energy

H - Hamiltonian

E_{ani} - anisotropy energy density

H_d - demagnetizing field

M - magnetization

N - demagnetizing factor

K_s - shape anisotropy

K_u - magnetocrystalline anisotropy

M_s - saturation magnetization

F - free energy

S - entropy

T - temperature

MSA - magnetic surface anisotropy

TOM- torsion oscillation magnetometry

σ_s - surface energy

K^{eff} - effective anisotropy constant

K_v^{eff} - effective volume anisotropy constant

K_s^{eff} - interface anisotropy constant

μ - magnetic dipole moment

τ_{eff} - effective torque

H_{eff} - effective field

G - Gilbert damping term

MRAM - Magnetoresistive random access memory

V_o - atomic volume

δ - skin depth

d_{ex} - exchange length

P_m - microwave power

H_o - external dc field

ΔH_{pp} - ferromagnetic resonance linewidth

α - magnetic damping

ESR - electron paramagnetic resonance

T_c - Curie temperature

t - tolerance factor

ζ - coherence epitaxy

ε_m - misfit strain

ε_c - in-plane compressive strain

P - pressure

σ_c - conductivity

TMR - tunnel magnetoresistance

MCE - magnetocaloric effect

ΔT_{ad} - adiabatic change in temperature

a - lattice constant

CPW - coplanar waveguide

VNA - vector network analyser

Q- quality factor

r- Mn -Mn distance

ξ - spin orbit coupling

ψ - angle between the magnetization and magnetic axis

θ and ϕ - polar angles of magnetic moment in the crystal axis frame

β - angle between the magnetization, M and surface normal, n

φ - azimuthal angle

Ψ and Ω - magnetization angles

η - angle between the external magnetic field and direction z normal to the film

K_i - anisotropy constants

H_s - stray field

τ - torque

λ - relaxation frequency

q - charge of electron